University of Freiburg

Master's Thesis

Transit times and storage properties of mesoscale catchments in Switzerland

Author:
Stefan Seeger

Supervisor:
Prof. Dr. Markus Weiler

A thesis submitted in fulfilment of the requirements for the degree of Master of Science in Hydrology

in the

Institute for Hydrology

January 2013

Declaration of Authorship

I, Stefan SEEGER, declare that this thesis titled, 'Transit times and storage properties of mesoscale catchments in Switzerland' and the work presented in it are my own. I confirm that:

- This work was done wholly or mainly while in candidature for a research degree at this University.
- Where I have consulted the published work of others, this is always clearly attributed.
- Where I have quoted from the work of others, the source is always given. With the exception of such quotations, this thesis is entirely my own work.
- I have acknowledged all main sources of help.
- Where the thesis is based on work done by myself jointly with others, I have made clear exactly what was done by others and what I have contributed myself.

Signed: _____

Date: _____

UNIVERSITY OF FREIBURG

Abstract

Faculty of Forest and Environmental Sciences
Institute for Hydrology

Master of Science in Hydrology

Transit times and storage properties of mesoscale catchments in Switzerland

by Stefan SEEGER

In this study the mean tracer transit times (MTT) and mean hydrological response times (MRT) of 24 hydrological catchments with differing geology and altitudes ranging from the Swiss Jura to the Swiss Alps have been determined. MTTs and MRTs were obtained through the calibration of lumped parameter convolution models and have been used to determine the total catchment storages and the dynamic storages, respectively, for each of the 24 catchments. MTTs have been estimated for with three different transfer functions: the exponential model, the gamma distribution and the two parallel reservoir (TPLR) model. The tracer data needed as input for the tracer convolution model was obtained by spatial interpolation of data of the Swiss ISOT-measurement network. The simulation performance for catchments with snow dominated runoff regimes could greatly be improved by the height level distributed application of a simple uncalibrated energy-balance based snow model.

Acknowledgements

First I would like to thank my supervisor, Prof. Dr. Markus Weiler, who introduced me to the topic of this study, induced some thought provoking impulses and supported me whenever I needed it.

Then I would like to thank Anita Gundel, who introduced me to the Drought-CH project, provided me with most of the data and information needed for this study, cross-read an early draft of this thesis and gave helpful feedback.

Furthermore, I would like to thank Barbara Herbstritt, who instructed me on the laboratory work, did conduct a good part of the isotope analyses herself and undertook the task of post-processing the isotope analysis results.

For their readiness to discuss and the offer to cooperate in order to improve the snow model, I would like to thank Dr. Stefan Pohl and Jacob Garvelmann.

Then I would like to thank Ernestine Lieder and Jakob Sohrt, who provided technical support and helped through constructive criticism.

I would also like to thank all the people involved in the Drought-CH project, whom I never really got to know and who contributed to the data collection which enabled this study: Maria Staudinger, Dr. Massimiliano Zappa, Dr. Manfred Sthli and many more.

Last but not least, I would like to thank my parents, who enabled me to pursue my academic studies to this point.

Contents

List of Figures

List of Tables

Abbreviations

MTT	**M**ean **T**ransit **T**ime
MRT	**M**ean **R**eaction **T**ime
TPLR	**T**wo **P**arallel **L**inear **Reservoirs**
ACO	**A**nt **C**olony **O**ptimization

Chapter 1

Introduction

1.1 Background

The Drought-CH project The Swiss national research program project Drought-CH was initiated as a reaction to the central European heatwave of 2003 and the ensuing water scarcity related ecological and socio-economic problems in Switzerland. One of the aims of Drought-CH is the characterization and early recognition of critical drought and low-flow conditions in Switzerland, which are expected to get more frequent as a consequence of climate change. Work package 3 of the Drought-CH project is dedicated to the quantification of the natural systems vulnerability and is the framework within which this study took place.

Drought types Kallis [2008] distinguishes between "meteorological droughts (abnormal precipitation deficits), agricultural droughts (abnormal soil moisture deficits), hydrological droughts (abnormal streamflow, groundwater, reservoir, or lake deficits), and water supply droughts (abnormal, temporary failures of supply to meet demands)". While meteorological droughts are the main reason for the occurrence of hydrological droughts, hydroenvironmental factors such as soil, snowpack and aquifer storage also decide whether abnormal precipitation deficits lead to a hydrological drought in a specific catchment. Catchments with high water storages are expected to be less sensitive in this respect. Therefore the knowledge of catchment water storages might help to improve the assessment of drought vulnerabilities.

1.2 Catchment water storage

Within a catchment, water can be stored as surface water, soil moisture, groundwater, snow or ice and in vegetation. While in situ measurements of these forms of water storage are possible, an accurate assessment on greater spatial scales is often difficult or impossible(Leblanc et al. [2009]). Repeated gravimetric measurements from Superconducting Gravimeters (SG), as done by Creutzfeldt et al. [2010], or the satellite based Gravity Recovery and Climate Experiment (GRACE) make it possible to asses spatially integrated changes in water storage(Andersen [2005]). However, the currently established SG technology is bound to the according infrastructure and is therefore limited to a few research sites. GRACE, on the other hand, has a global scope but the resulting spatial and temporal resolutions are rather coarse, limiting its use to the study of major river basins(Leblanc et al. [2009], Zaitchik et al. [2008]). Both gravimetric methods only detect storage changes in comparison to earlier measurements and cannot answer the question of total water storage in a system.

1.2.1 Tracer based total storage estimation

A more promising approach to asses the total water storage on the catchment scale is based on the determination of the mean transit time (MTT) of a tracer. Under the assumption of a well mixed catchment storage without immobile zones, the mean total storage size can be computed as the product of MTT and mean discharge(McGuire [2005]). A comprehensive review on the MTT issue was done by McGuire and McDonnell [2006]. Without giving explicit recommendations for minimum data record lengths, McGuire and McDonnell [2006] point out that estimates for MTTs become less reliable when the input and output data records are rather short in comparison to the MTT, as tracer recovery within the analysed timespan might be too small to determine the MTT.

While there are a lot of studies which focus on transit time distributions (TTDs) and/or MTTs (e.g. [McGuire, 2005, Hrachowitz et al., 2010, Mueller et al., 2012, Weiler, 2003, Dunn et al., 2010, Roa-García and Weiler, 2010, Fenicia et al., 2010, Birkel et al., 2011]), not all of them report the according storage measures. McNamara et al. [2011] compared the storages of five catchments in Scotland, Sweden and the USA and reports mean total storages ranging from 80 to 769 mm, but it has to be noted that different methods were

used to obtain these storage values. Hrachowitz et al. [2010] used a lumped convolution integral model to estimate TTDs and MTTs for 14 Scottish catchments. Soulsby et al. [2011] reported the according total storage estimates for the 12 catchments with reliable MTT estimates to range from 300 to 2500 mm.

1.2.2 Relations between mean transit time and catchment properties

Whilst MTTs and the according total catchment storage estimates appear to be meaningful catchment characteristics, the required tracer data records are relatively hard to obtain and usually limited to selected research catchments. Therefore, it would be desirable to identify relations between MTTs and other, more readily available, catchment characteristics, such as soils, geology and geomorphology.

McGuire [2005] investigated seven catchments with areas ranging from 0.085 to 62.42 km^2 within an elevation range from 418 to 1630 m. All catchments were located within the H.J. Andrews Experimental Forest in the central western Cascades of Oregon, USA. The dominating bedrock of all catchments was reported to be of volcanic origin and the soils show high infiltration rates and high drainable porosity. The MTTs were estimated by using lumped convolution integral models and $\delta^{18}O$ data and ranged from 0.8 to 3.3 years. For these seven catchments, McGuire [2005] found strong correlations between the estimated MTTs and morphological catchment characteristics derived from a digital elevation model (DEM) with a resolution of 10 m. The correlation between MTTs and mean catchment slopes had an r^2 of 0.78. The ratio L/G, where L is the median length of all flowlines within a catchment and G the median gradient of these flowlines, showed the best correlation to MTTs($r^2 = 0.91$).

Hrachowitz et al. [2010] and Soulsby et al. [2011] investigated 14 Scottish catchments with areas ranging from 0.5 to 1800 km^2, mainly located in the Scottish highlands. Mean annual precipitation sums ranged from less than 1000 to over 2000 mm and soils varied from highly responsive to freely draining. The MTT estimates for 12 of the 14 studied catchments ranged from 61 days to 6.6 years, while the MTTs for the remaining two catchments were estimated to be at least 13 and 16 years. There

was no significant correlation between hillslope gradients and MTTs in this study. High correlations with MTTs were found for soil drainage classes and drainage densities.

Mueller et al. [2012] studied the relation between MTTs and vegetation cover for four micro catchments in the Ursern valley in the Swiss Alps, with areas ranging from 0.2 to 0.56 km^2 and elevations between 1500 and 2500 m. MTTs were estimated to range from 1.2 to 1.8 years. No significant correlations bewteen MTTs and topographic characteristics could be found.

1.3 Water isotopes as hydrological tracers

1.3.1 Water isotopes

Each water molecule (H_2O) consists of two hydrogen atoms (H) and one oxygen atom (O). Different isotopes, i.e. atoms with the same number of protons but differing numbers of neutrons, exist for both of these elements and are listed in table 1.1. Except for the radioactive Tritium, all of these isotopes are stable. Naturally the listed isotopes occur next to each other with a certain abundance.

TABLE 1.1: Water isotopes and their characteristics [Dingman [2002]]

Formula	Name	Natural Abundance[%]	Relative Mass
^1H	Protium	99.985	1.008
^2H	Deuterium	0.015	2.014
^3H	Tritium	< 0.01	3.016
^{16}O	^{16}O	99.76	15.995
^{17}O	^{17}O	0.04	16.999
^{18}O	^{18}O	0.2	17.999

1.3.2 The δ-notation

Instead of directly stating the abundance of the stable water isotopes in a sample, the so called δ-notation(Craig [1961]) is used, which is based on the ratio of the amount of

a rarer isotope I_{rare} to that of the most abundant isotope of an element $I_{abundant}$:

$$R = \frac{I_{rare}}{I_{abundant}} \tag{1.1}$$

This ratio has to be determined for the sample and a standard, like the Vienna standard mean ocean water (VSMOW), before the δ-value can be determined as:

$$\delta = (\frac{R_{\text{sample}}}{R_{\text{VSMOW}}} - 1) \times 1000‰ \tag{1.2}$$

Positive δ values indicate that, compared to the standard, the sample is enriched in the considered isotope while negative values indicate depletion.

1.3.3 Isotope fractionation

The ratios of the abundances of ^{18}O to ^{16}O and ^{2}H to ^{1}H are altered through the hydrological cycle. While different isotopes of one element show the same chemical properties, they have different masses, what leads to higher melting and boiling points for water molecules containing heavier isotopes of H and O compared to $^{1}H_2{}^{16}O$ molecules(Hölting and Coldewey [2005]). Those physical differences are the reason for a fractionation, taking place at every partial phase transition and leaving the volume fraction in the energetically lower phase (ice, water) enriched in heavy isotopes and the volume fraction in the energetically higher phase (water, vapour) depleted in heavy isotopes. In regard to condensation from water vapour, this is also described as Rayleigh-Distillation.

1.3.4 Stable isotopes in precipitation

Considering the stable water isotopes in precipitation, the following effects are observed:

1.3.4.1 Amount effect

There is a negative correlation of δ values against mean monthly precipitation amounts which can be found all year round for tropical stations and during the summer time in mid latitudes(Dansgaard [1964]).

1.3.4.2 Continental effect

Precipitation gets depleted in heavier isotopes the farther away from the vapour source (in most cases the ocean) it occurs(Dansgaard [1964]).

1.3.4.3 Temperature effect

For high latitude non-continental precipitation, there is a simple linear correlation between the annual mean values of the surface temperature and the annual mean $\delta^{18}O$ values.(Dansgaard [1964]).

1.3.4.4 Seasonal effect

For higher latitudes there is a clear seasonal variation of δ values, with heavier precipitation in the summer and lighter precipitation in the winter season(Dansgaard [1964]).

1.3.4.5 Altitude effect

With increasing altitude an increasing depletion in heavy isotopes can be observed. Leibundgut et al. [2009] point out, that locally other effects, as mixing of air masses, can be important factors which determine the precipitation's isotopic composition, which is why the altitude effect should be checked with local data.

1.3.5 Application as tracer

As the fractionation only occurs during phase transitions, the δ-values of water usually do not change once it reached a point where no evaporation takes place. Solely a mixture of waters can cause a change in δ-values. This makes stable water isotopes convenient natural tracers for hydrological purposes (Leibundgut et al. [2009]). Under the assumption of a well mixed reservoir, the dampening of the seasonal variation of precipitation δ-values can be used to determine the mean transit time of water in that reservoir.

Chapter 2

Data and Methods

2.1 Catchments

Landcover In this study 24 catchments distributed across the Swiss Plateau and the Swiss Alps (see figure 2.1) have been analysed. Their areas, mean heights and landcover distributions are listed in table 2.1. The investigated research catchments' mean heights lie between 472 and 2386 m above sea level and their areas range from 0.77 to 351 km^2. The landcover distributions listed in table 2.1 (derived from CLC2006[1] 100 m raster data) seem to be correlated with the catchment heights. Artificial and agricultural areas at lower heights (under 800 m), grasslands, pastures and forests at mid altitudes(800 - 1400 m) and grasslands and sparsely vegetated areas above 1700 m. The catchments were selected for the criteria: least possible human influence, glaciers covering less than 5% of the catchment are and data availability.

Geology and Pedology [2] Underlying geology and pedology vary between and within the catchments. The catchment *Ergolz Liestal* lies in the Swiss Jura, which consists of lime- and marlstone. Most of the catchments are distributed across the Swiss Plateau, where sedimentary layers of molasse and flysch are dominant. The highest catchments are found in the Swiss Alps, where crystalline bedrock and limestone are prevailing.

[1] Corine Land Cover 2006 by the European Environment Agency (EEA), http://www.eea.europa.eu/data-and-maps/data/corine-land-cover-2006-raster

[2] Information obtained from the FOEN-website: http://www.hydrodaten.admin.ch/en/

TABLE 2.1: Mean catchment heights, catchment areas and landcover distributions of the 24 studied catchments

Mean Height [m]	Min Height [m]	Max Height [m]	Area [km^2]	
2369	1663	3139	43.2	Dischmabach_Davos
2364	1519	3160	26.9	Ova_da_Cluozza_Zernez
1986	881	2908	23.9	Riale_di_Calneggia_Cavergno
1852	1293	2742	28.8	Allenbach_Adelboden
1719	487	3260	107.9	Schaechen_Buerglen
1359	1117	1650	0.7	Erlenbach
1336	1092	1508	0.9	Luempenenbach
1335	1038	1540	1.6	Vogelbach
1301	768	2500	88.2	Sitter_Appenzell
1285	743	2216	127	Emme_Eggiwil
1154	845	1894	46.5	Alp_Einsiedeln
1068	554	2184	351.2	Sense_Thoerishaus
1037	681	2087	187.9	Ilfis_Langnau
1037	566	2152	55.4	Guerbe_Burgistein
999	827	1495	31.6	Biber_Biberbrugg
991	731	1542	54.1	Roethebach_Eggiwil
815	748	938	0.9	Oberer_Rietholzbach
794	671	938	3.2	Rietholzbach_Mosnang
760	598	1100	60.3	Langeten_Huttwil
679	447	926	105	Mentue_Yvonand
648	467	1036	76.8	Murg_Waengi
635	519	1092	55.6	Aabach_Moenchaltorf
584	305	1165	261.2	Ergolz_Liestal
472	408	560	50	Aach_Salmsach

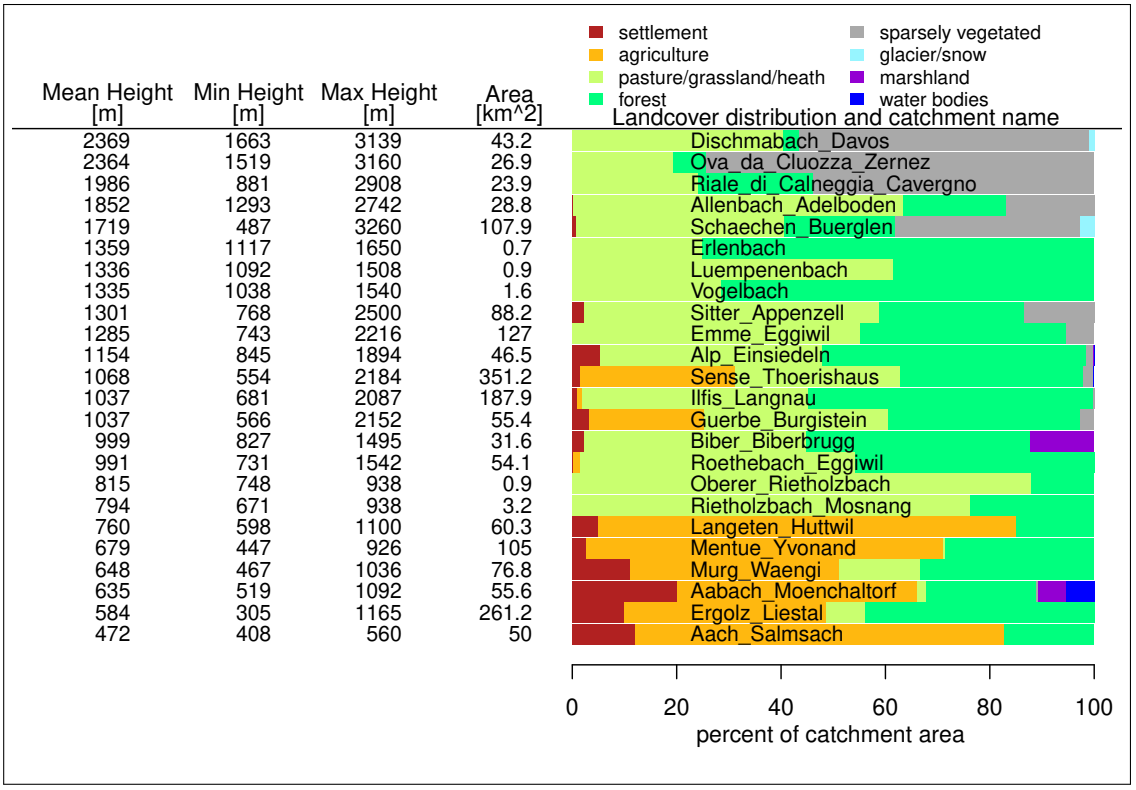

Phenomena related to karst formation might be relevant for the catchments *Ergolz Liestal*, *Sitter Appenzell* and *Ova da Cluozza Zernez*. Rather marginal karst occurrences can be found within the headwaters of the catchments *Allenbach Adelboden*, *Alp Einsiedeln* and *Sense Thoerishaus*. Moraines of former glacial periods are superimposed on the underlying geology in parts of most of the catchments. In the lower regions of the catchment *Dischmabach Davos* heavy moraines form a notable layer with high water storage capacity.

The prevailing soil types are depicted in figure 2.1. The north-western strip of Rendzinas coincides with the Swiss Jura, while the Swiss Plateau is mostly covered by Luvisols and Cambisols. In the Swiss Alps, Rendiznas and Lithosols are the dominant soil types. However, it is important to note, that this is a gross simplification and does not account for the actual variety of soil types within the catchments. Average soil storage capacities lie within a range of 14 mm (*Riale di Calneggia Cavergno*) to 74 mm (*Langeten Hutwil*).

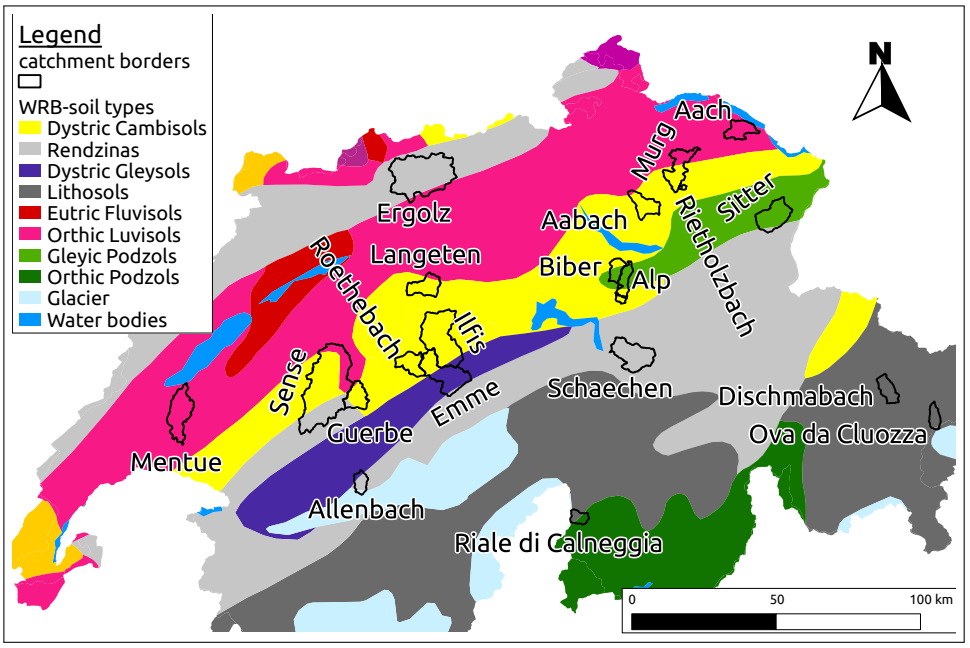

FIGURE 2.1: Map of the prevailing soil types across the study area [source:FAO digital soil map of the world] and catchment borders

2.1.0.1 Runoff Regimes

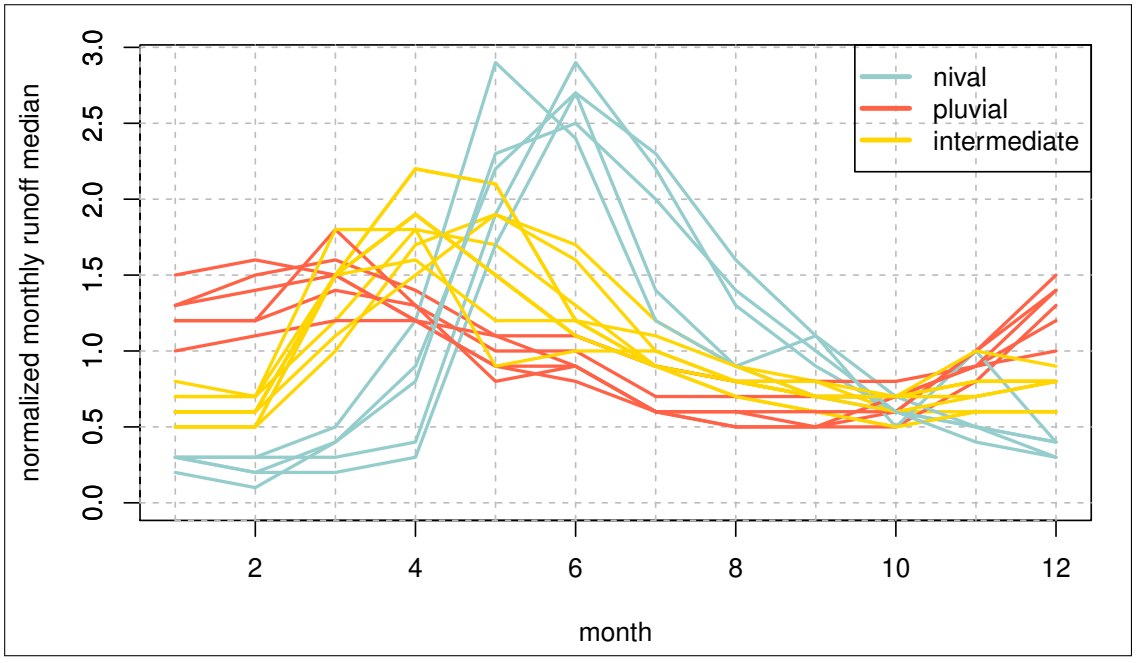

FIGURE 2.2: Normalized average monthly runoff values for each of the studied catchments

Figure 2.2 shows the normalized average runoff values of the 24 research catchments included in this study. They can be assigned to three runoff regime types: Nival runoff

regimes (blue in figure 2.2) show a clear runoff minimum through fall and winter, caused by snow accumulation, and a distinct runoff maximum in May to June, caused by melt of the acumulated snow. The main influence on the seasonal cycle of pluvial runoff regimes (red in figure 2.2) consists of the seasonal differences in evapotranspiration and higher winter precipitation, resulting in a weak maximum in winter and a weak runoff minimum during late summer and early fall. Intermediate runoff regimes (yellow in figure 2.2) between the two aforementioned regime types show a weaker, but still recognizable, influence of snow accumulation and melt. Runoff regime types primarily are a consequence of climatic conditions, mostly precipitation and temperature. Due to the relatively small extent of the study area, the most notable climatic differences result from the altitude differences within the study area. Thus, the catchments with mean heights above 1700 m A.S.L. have nival runoff regimes, the catchments with mean elevations below 900 m have pluvial runoff regimes and the intermediate are found in between these heights (see figure 2.3)

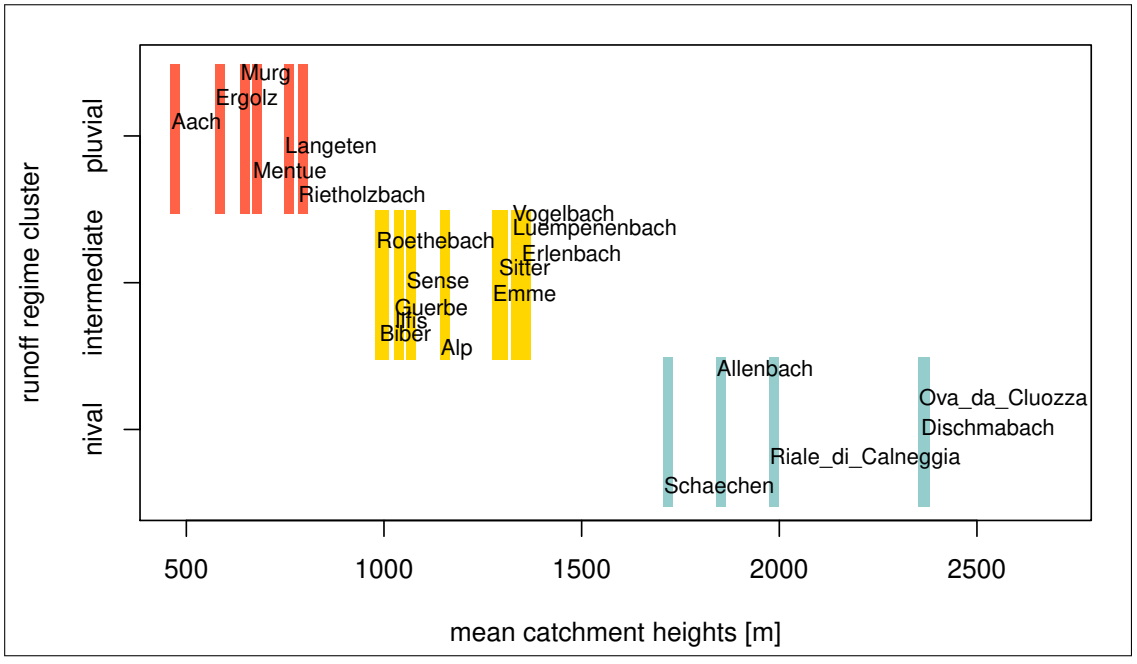

FIGURE 2.3: runoff regimes plotted against mean catchment heights

2.2 Data

2.2.1 Climate Data

The climate data used in this work(precipitation, temperature, relative air humidity, wind speed, global radiation) was provided by the PREVAH working group [Viviroli et al., 2009], which is a climate data processing framework to simulate hydrological processes for catchments all over Switzerland. PREVAH obtains climate data of Swiss measurement sites directly from MeteoSwiss(the national meteorological service of Switzerland) and other data sources. The site data gets spatially interpolated and maps for each climate parameter are created for each modelling time step. Shapefiles containing the catchment borders were used to obtain daily average values for 100 m height levels for each catchment.

2.2.2 Runoff Data

Most runoff data was obtained by the Swiss Federal Office for the Environment (FOEN). Runoff data for the catchments *Luempenenbach*, *Erlenbach* and *Vogel* was obtained from the *Swiss Federal Institute for Forest, Snow and Landscape Research* (WSL). Additional runoff data for the catchment *Roethebach* provided by the Amt für Abwasser und Umwelt (AWA) of the Swiss Canton Berne.

2.2.3 Runoff Isotope Data

100 ml runoff samples from the catchments of interest were taken at bi-weekly intervals from mid 2010 to mid 2012. The samples were analyzed for stable water isotopes with a PICARRO cavity ringdown spectrometer at the *Institute for Hydrology* (IHF) at the University of Freiburg im Breisgau from end of 2011 to mid 2012.
Additional runoff isotope data for the catchment *Rietholzbach Mosnang* and its subcatchment *Oberer Rietholzbach* was retrieved from the Institute for Atmospheric and Climate Science (IAC) of the Swiss Federal Institute of Technology Zurich. Therefore, the available runoff isotope time series for those two catchments extent further into the past, although newer runoff isotope measurements for the subcatchment *Oberer Rietholzbach* are missing.

2.2.4 Precipitation Isotope Data

The National Network for the Observation of Isotopes in the Water Cycle (ISOT) of the *Federal Office for the Environment* (FOEN) of Switzerland contains 13 sites at which stable water isotopes ($\delta^{18}O$ and $\delta^{2}H$) in the precipitation are measured for monthly periods. Additional monthly data from the site Konstanz of the *International Atomic Energy Agency*'s (IAEA) *Global Network of Isotopes in Precipitation* (GNIP) was integrated into the ISOT data set. The considered timespan begins in July 1994 and ends in October 2011, predominantly incorporating twelve sites' values per month, never less than ten.

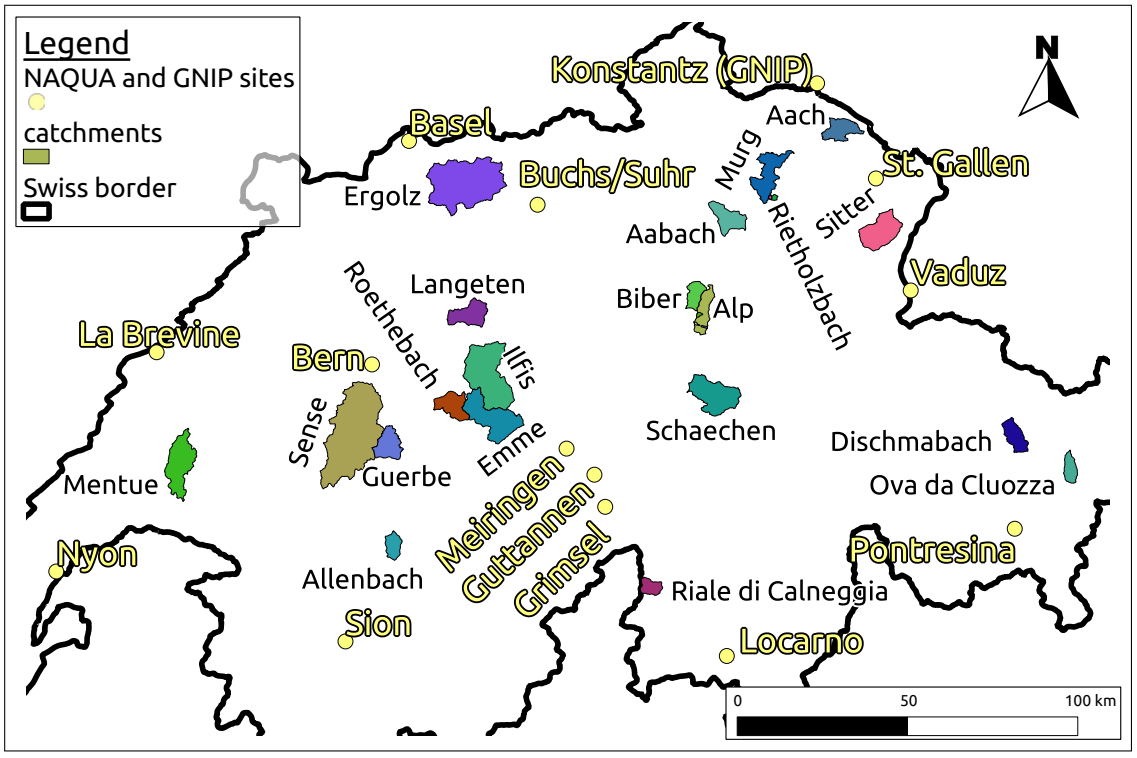

FIGURE 2.4: Map of the precipitation isotope sampling sites (yellow labels) and catchments (black labels); *Vogelbach*, *Erlenbach* and *Luempenenbach* are subcatchments of *Alp*

2.2.5 Interpolation of Isotope Data

In the first step the respective value of the measurement site closest to the catchment was reduced to it's theoretical sea level value by the respective average monthly height-gradient, to obtain monthly isotope concentrations in precipitation for a specific catchment, year and month:

$$i_{SYM} = I_{SYM} - h_S \times g_{\overline{Y}M} \tag{2.1}$$

where I_{SYM} is the isotope concentration value for measurement site S in year Y and month M (ranging from 1 to 12), i_{SYM} is the theoretical sea level equivalent of I_{SYM}, h_S is the measurement site's height above sea level and $g_{\overline{Y}M}$ the respective month's average height-gradient. The average monthly height gradients were computed out of the values of the three measurement sites *Meiringen*, *Guttannen* and *Grimsel*, which lie along a transect in the Berneese Alps between 632 and 1950 m above sea level (see the map in figure 2.4). It was assumed that these average monthly height gradients are representative for the whole study area. Then the catchment's theoretical isotope concentration in precipitation at sea level for a specific month (i_{CYM}) were be computed as:

$$i_{CYM} = i_{SYM} - i_{S\overline{Y}M} + i_{C\overline{Y}M} \tag{2.2}$$

where $i_{S\overline{Y}M}$ and $i_{C\overline{Y}M}$ are the average sea level precipitation isotope concentrations of measurement sites and catchments for the respective month. Finally the catchment's isotope concentration in precipitation for the desired month (I_{CYM}) was computed by adding the product of the height-gradient and the mean catchment height h_C:

$$I_{CYM} = i_{CYM} + h_C \times g_{\overline{Y}M} \tag{2.3}$$

While the values for i_{SYM} and $i_{S\overline{Y}M}$ could easily be computed from the original I_{SYM} values, $i_{C\overline{Y}M}$ values were obtained by spatial interpolation of $i_{S\overline{Y}M}$ values. This was achieved by kriging[Delhomme, 1978], using *t*he R(see2.4) *gstat*-package[Pebesma, 2004].

2.3 Models

2.3.1 TRANSEP

2.3.1.1

The time series variant of the *trans*fer function hydrograph *sep*aration model[*TRANSEP*-Weiler, 2003], was chosen to model the catchments' hydraulic reactions and tracer signals. The approach of *TRANSEP* is to reduce the precipitation amount by means of a non linear rainfall loss module based on a wetness index, accounting for effects of evapotranspiration without explicitly modelling it, and then convolute the effective precipitation with a transfer function to retrieve the resulting runoff amounts. The tracer concentration in the precipitation is weighted by the effective precipitation amount and gets convoluted by a second transfer function to simulate the runoff tracer concentration. This basic approach has proven to work sufficiently well under a range of conditions [McGuire, 2005, Weiler, 2003, Roa-García and Weiler, 2010, Hack, 2010]. However, as can already be expected, Hack [2010] found that the hydrological behaviour of catchments characterized by snow accumulation and melt cannot be predicted by the basic structure of the *TRANSEP* approach.

2.3.1.2 Rainfall Loss Module

While the *TRANSEP* framework is not bound to any particular method for computation of effective precipitation, in this study solely the approach described by Jakeman and Hornberger [1993] was used. It is based on a storage index s_k which is computed iteratively for each timestep k:

$$s_k = c \times r_k + (1 - \tau_w^{-1}) s_{k-1} \tag{2.4}$$

where c is the increase in storage index per unit of precipitation, r_k is the rainfall amount of timestep k and τ_w is the persistence of the storage index, determining how fast the index drops on days without precipitation. To account for fluctuations in evapotranspiration, the storage index persistence τ_w is adjusted by a temperature dependent function:

$$\tau_w(t_k) = \tau_w \times exp[(20 - t_k)f] \tag{2.5}$$

where t_k is the timestep's temperature in degrees Celsius, τ_w the storage index persistence at 20 degrees Celsius and f is a temeperature modulation parameter which determines how $\tau_w(t_k)$ changes with temperature
The storage index is then used to compute the excess rainfall u_k for each timestep using the formula:

$$u_k = r_k * s_k \tag{2.6}$$

Thus, the rainfall loss module requires time series of precipitation and temperature and has three parameters (c, τ_w and f) which need to be calibrated.

2.3.1.3 Linear Convolution Module

The runoff Q for a certain time step t is described by a convolution of the hydraulic transfer function $h(\tau)$ with all preceding effective precipitation values p_{eff} (Weiler [2003]):

$$Q(t) = \int_0^t h(\tau) p_{\text{eff}}(t-\tau) d\tau \tag{2.7}$$

. The tracer concentration in runoff $C_Q(t)$ is computed in a similar way, but the input tracer concentrations C_P are weighted by the respective effective precipitation amounts and convoluted by a tracer transfer function $g(\tau)$ (Hrachowitz et al. [2010], Weiler [2003], Stewart and McDonnell [1991]):

$$C_Q(t) = \frac{\int_0^t g(\tau) p_{\text{eff}}(t-\tau) C_P(t-\tau) dt}{\int_0^t g(\tau) p_{\text{eff}}(t-\tau) d\tau} \tag{2.8}$$

2.3.1.4 Transfer Functions

A variety of transfer functions can and have been used to convolute precipitation or tracer concentration input time series to obtain runoff, respectively runoff tracer concentration time series [McGuire, 2005, Hrachowitz et al., 2010, Weiler, 2003, Roa-García and Weiler, 2010, Hack, 2010, Malozewski and Zuber, 1982, Kirchner et al., 2000]. Whenever applied, the *Two parallel linear reservoirs* (TPLR,[Weiler, 2003]) transfer function performed as the best or one of the best transfer functions. The formula for the TPLR transfer function is:

$$h(\tau) = g(\tau) = \frac{\phi}{\tau_f} exp(-\frac{\tau}{\tau_f}) + \frac{1-\phi}{\tau_s} exp(-\frac{\tau}{\tau_s}) \tag{2.9}$$

where τ is the time, $h(\tau)$ a hydraulic transfer function and $g(\tau)$ a tracer transfer function. τ_f and τ_s are the mean residence times of a fast and a slow responding reservoir, respectively. The parameter ϕ determines how much of the input signal is going into the fast reservoir, leaving the remaining fraction $1 - \phi$ for the slow reservoir. In this work, the TPLR is the only transfer function used as h_τ.

For the prediction of tracer concentrations two further, widely used, transfer function are used. The first one is the classical exponential transfer function after Malozewski and Zuber [1982]:

$$g(\tau) = \frac{1}{\tau_m} exp(frac - \tau\tau_m) \tag{2.10}$$

where the only parameter τ_m equals the mean transit time. The second additional transfer function is the two parameter gamma distribution after Kirchner et al. [2000]:

$$g(\tau) = \frac{\tau^{\alpha-1}}{\beta^\alpha \Gamma(\alpha)} e^{-\tau/\beta} \tag{2.11}$$

where Γ is the gamma function, α is a form parameter and β a scale parameter. The mean transit time of the gamma distribution transfer function can be computed as product of α and γ. Of those three transfer functions the exponential transfer function is the simplest. Provided that transit times through the unsaturated zone are negligible, it would result from an unconfined aquifer with uniform hydraulic conductivity and porosity(McGuire and McDonnell [2006], Malozewski and Zuber [1982]). Since the exponential transfer function has only one parameter, this one parameter can be identified fast and precisely. Transfer functions with more parameters (two for the gamma distribution, three for the TPLR) have more degrees of freedom and therefore are more flexible. Both, the gamma distribution as well as the TPLR, can take the form of the exponential transfer function, when their parameters are set accordingly. Additionally they can account for different flow path distributions with shorter and longer flowpaths. The downside of the higher flexibility is the increased difficulty to identify the parameter values, i.e. increased computing time for the calibration and possibly high uncertainties. For this reason, McGuire [2005] finally focused on the MTTs implied by the exponential transfer function. Hrachowitz et al. [2010] and associated studies (e.g. Soulsby et al. [2011]) focus on MTTs obtained by gamma distribution transfer functions.

The gamma distribution has proven to yield similar results as the TPLR when used for the estimation of MTTs and is more widely used than the TPLR(Hrachowitz et al.

[2010]).

2.3.1.5 Parameter Optimization I:*Ant Colony Optimization* (*ACO*)

The parameter optimization follows a modified version of the *ACO* algorithm after Abbaspour et al. [2001]. In a series of Monte Carlo simulations random parameter sets are chosen from within the given parameter ranges. The simulations are evaluated and the parameter ranges are constrained successively.

The parameter ranges are partitioned into a number of strata, where a higher number of strata should lead to convergence in fewer iterations, while the number of model runs per iteration increases with the rate p^s, with p being the number of parameters to optimize and s the number of strata. If the number of strata is set too high, the computing time quickly becomes rampant, hence Abbaspour et al. [2001] proposed to choose random subsets amounting to 10% of the total set of possible parameter combinations. However, this still does not stop the rapid growth of the number of simulations to run with increasing numbers of parameters or strata.

After all simulations of an iteration have been run, the ranges for each parameter are updated. In a first step, a trail intensity τ_u is assigned to each parameter combination u:

$$\tau_u = \begin{cases} exp(4.6(\frac{v_u - v_{cr}}{v_{min} - v_{cr}})), & v_u \leq v_{cr} \\ 0, & v_u > v_{cr} \end{cases} \tag{2.12}$$

where v_u is the value of an objective function for the parameter combination u. The objective function has to yield smaller values for better simulations. The smallest objective function value reached in the current iteration is v_{min} and v_{cr} is a critical objective function value, above which the trail intensity is set 0. The closer the critical value v_{cr} is to v_{min}, the faster the algorithm converges, but also the higher is the probability of missing the global optimum. The critical value is computed dynamically for each iteration:

$$v_{cr} = v_{min} + c_T \frac{\sigma_v}{\mu_v} \tag{2.13}$$

where σ_v and μ_v are the standard deviation and the mean value of all objective function values of the current iteration. The constant c_T is set to 0.5.

The trail intensities are then used to assign an intensity value ϕ_{ij} to each parameter stratum β_{ij}, with i being a specific parameter and j one of its value strata:

$$\phi_{ij} = \sum_{\text{u } \epsilon \text{ parameter combinations containing } \beta_{ij}} \tau_u \tag{2.14}$$

Then, a score value S_{ij} is computed for each stratum:

$$S_{ij} = \frac{(\phi_{ij})^A (\sigma_{ij})^N}{\sum_i \sum_j (\phi_{ij})^A (\sigma_{ij})^N} \tag{2.15}$$

S_{ij} = score value of β_{ij}

ϕ_{ij} = intensity value for β_{ij}

σ_{ij} = standard deviation of all objective function values involving β_{ij}

As can be seen, not only the trail intensity ϕ_{ij} is used to calculate a stratum's score, but also the standard deviation of the stratum's trails σ_{ij}. This accounts for the strata's sensitivities and prevents strata with high trail variabilities from being eliminated too early.

The parameters A and N determine the influence of ϕ_{ij} and σ_{ij}, respectively. Abbaspour et al. [2001] set $A = 1$ and

$$N = c_n \frac{\sigma_{ij}}{\mu_{ij}} \tag{2.16}$$

c_n = a constant set to 0.3

μ_{ij} = mean trail intensity value of for β_{ij}

Based on the strata's score values, the parameter ranges are updated. Low score values of strata at the borders of a parameter range lead to a constriction of the parameter range. If the best scoring parameter stratum is at the upper or lower border of the parameter range, the parameter range is extended in that direction.

This is repeated over several iterations, until a stopping rule is satisfied. In this work, the stopping rules are:

(1) v_{max}-$v_{min} < D_s$

(2) maximum number of iteration reached

(3) no changes of parameter ranges between two iterations

Stopping rule (1) is meant to stop the algorithm as soon as the difference between the worst and the best objective function value of all simulations (v_{max} and v_{min}) of an iteration is smaller than a significant difference D_s. When defining this significant difference, the nature of the used objective function has to be taken into account. For the NSE-like objective functions used in this work, D_s was set to 0.05.
Deviating from the proposed choice of discrete parameter values, i.e. each stratum is only represented by its middle value, this work tried another approach by choosing random parameter values from within the strata's value ranges.

2.3.1.6 Parameter Optimization II: Uncertainty

Abbaspour et al. [2001] proposed to stop the algorithm as soon as the interval between the 2.5 to 97.5 percentiles of all simulated values includes 95% of all observed values plus their errors. While this stopping rule theoretically yields reasonably defined parameter ranges, it actually only does so, when the errors are known and a high number of strata is used. In case the number of strata is low (what reduces the number of simulations to run greatly), one iteration might come close to the aforementioned 95% threshold while the next iteration might constrain the parameter ranges so far, that far less than 95% of the observations lie within the confidence intervals of the simulations. At this point the algorithm stops and the parameter ranges actually represent an unknown, narrower than 95%, confidence interval[3].
Instead of the 95% confidence interval stopping rule, the simpler stopping rules described at the end of 2.3.1.5 were implemented. Thus, depending on the parameter sensitivities and on which stopping rule was met to end the ACO-algorithm, the parameter ranges of the last iteration are not necessarily a good representation of the possible parameter ranges. To get a better idea of the acceptable parameter ranges, the results of all ACO-iterations for one calibration are considered. First a threshold objective function value,

[3] An example for this case can be seen at page 72 of Hack [2010], included in Appendix B

v_T is set:

$$v_T = \begin{cases} v_{50\%}(I_{n-1}), \text{ if stopping rule 1 (see end of 2.3.1.5) was met} \\ v_{50\%}(I_n) \quad \text{, if stopping rule 1 was not met and } v_{50\%}(I_n) \leq v_{1\%}(I_1) \\ v_{1\%}(I_n) \quad \text{, if stopping rule 1 was not met and } v_{50\%}(I_n) > v_{1\%}(I_1) \end{cases} \tag{2.17}$$

where $v_{50\%}(I_{n-1})$ is the median objective function value of the iteration before the final iteration, $v_{50\%}(I_n)$ the median of the objective function values of the final ACO-iteration and $v_{1\%}(I_1)$ the one percentile value of all objective function values of the first ACO-iteration. The three cases in equation (2.17) should account for all possible developments during the ACO-algorithm. The first case would be a clearly converging calibration (or, theoretically also possible: a calibration where the parameter values do not matter, since all combinations lead to similar objective function values). In the second case, the final iteration has significantly better objective function values than the first iteration, which indicates that a constriction of the parameter ranges does lead to better simulations, even tough the final parameter ranges still allow for a wide range of objective function values. The third case covers calibrations where the final iteration did not significantly surpass the first iteration.

Then the objective function values of all parameter combinations from all ACO-iterations are compared to v_T. The ranges of all parameter combinations with objective function values smaller than v_T are taken to define a search range R_S for each parameter. Then simulations with random parameter combinations from within the ranges given by R_S are run and their objective function values are determined until a certain number M of simulations with objective function values smaller than $v_{5\%}(I_n)$ (5% percentile of the objective function values of the final ACO-iteration) has been found. Out of those M near to best simulations the possible ranges and median values of all parameters of interest are determined. As parameters of interest count:

$ET_{\overline{Y}}$: average yearly sum of evapotranspiration

RT: mean hydraulic reaction time

TT: mean tracer transit time

where $ET_{\overline{Y}}$ is partly determined by an calibration invariant sublimation component (computed by the snow model) and mostly by the parameters of the rainfall loss module. RT and TT are determined by the parameters used for the hydraulic transfer function $h(\tau)$ and the tracer concentration transfer function $g(\tau)$, respectively.

2.3.1.7 Objective Functions

The parameter optimization algorithm requires an objective function which can be used to evaluate and compare the goodness of different simulations, in order to identify good parameter sets and find an optimal solution.

An often used measure of model goodness in hydrological modelling which accounts for the data variability is the Nash-Sutcliffe-Efficiency NSE [Nash and Sutcliffe, 1970, Legates and McCabe, 1999]. The NSE is the mean square error of the prediction divided by the variance of the observed values:

$$\mathrm{NSE} = 1 - \frac{\sum_{i=1}^{n}(O_i - P_i)^2}{\sum_{i=1}^{n}(O_i - \overline{O})} \tag{2.18}$$

where O_i and P_i are the observed and predicted values of time step i and $\overline{O}$ is the mean of all observed values. A NSE value of 1 indicates perfect accordance of observed and predicted values, whereas a NSE of 0 means the simulated values are as reliable for prediction as the mean value of all observations. To weaken the influence of the highest values and to increase the influence of the lower value ranges, the observed and predicted data can be logarithmized before computing the NSE, which form now on will be referred to as logNSE.

To ensure that a runoff simulation produces plausible values, the relative absolute volume error (RAVE) was introduced:

$$\mathrm{RAVE} = \frac{|\sum_{i=1}^{n}(O_i - P_i)|}{\sum_{i=1}^{n} O_i} \tag{2.19}$$

The RAVE returns 0, when the total sum of all predicted runoff values equals the total sum of all observed runoff values and bigger values for all over- and underestimations. The temporal distribution of the predicted values does not have to be in agreement with the observed values, as long as the total sums are equal. Therefore the RAVE alone is not enough to evaluate the goodness of a simulation and it should only be used to

complement another objective function which accounts for the qualitative distribution of the values (e.g. the NSE) when precipitation correction factors have to be calibrated (see 2.3.3 and 2.3.4.3). The final objective function used to evaluate the runoff simulations is a combination of differently weighted objective functions which account for different aspects of the prediction:

$$\text{obFun}_{\text{hyd}} = \frac{2 \times (1 - \text{NSE}) + 3 \times (1 - \text{logNSE}) + \text{RAVE}}{5} \tag{2.20}$$

In the stated form, $\text{obFun}_{\text{hyd}}$ returns 0 for perfect predictions and bigger values for worse predictions.

As there were some uncertainties concerning the tracer input values, the tracer model predictions could not directly be evaluated. Instead, predicted and observed values had to be normalized by their respective median values:

$$\text{obFun}_{\text{trac}} = 1 - \text{NSE}(O - O_{\text{MEDIAN}}, P - P_{\text{MEDIAN}}) \tag{2.21}$$

Next to the values of $\text{obFun}_{\text{trac}}$, a tracer concentration prediction bias was computed as:

$$\text{bias}_{\text{trac}} = P_{\text{MEDIAN}} - O_{\text{MEDIAN}} \tag{2.22}$$

During the calibration of the tracer model $\text{bias}_{\text{trac}}$ was not considered, solely $\text{obFun}_{\text{trac}}$ had to be minimized.

2.3.2 Snow Model *ESCIMO*

2.3.2.1

To encounter the problem of poor performance of the *TRANSEP*-framework when modelling catchments which are influenced by snow accumlutaion and melt processes, a simple energy balance based snow model is applied before *TRANSEP*. Due to a lack of further information, the snow model uses the same standard parametrization for each catchment, disregarding land cover differences.

The snow model used in this work is a modified implementation of *ESCIMO* (*E*nergy balance *S*now *C*over *I*ntegrated *MO*del, Strasser and Marke [2010]). The *ESCIMO* version the used snow model is based on, *ESCIMO.spread*[4], consists of a spreadsheet file containing several sheets for input data, computations and visualisation of results. While *ESCIMO.spread* requires hourly input values for air temperature, precipitation amount, wind speed, relative air humidity, incomming shortwave radiation and incoming longwave radiation, only daily values were available for this work and longwave radiation data was not available at all. Therefore some modifications had to be made before *ESCIMO* could be applied.

2.3.2.2 Empirical Relation for Incoming Longwave Radiation

The missing data for incoming longwave radiation was filled with estimated values based on an empirical relation stated by Sicart and Pomeroy [2006]. The basic equation used to estimate incoming longwave radiation L_0 is:

$$L_0 = \varepsilon_{clear} F \sigma T^4 \tag{2.23}$$

where ε_{clear} is the clear-sky emissivity, F the increase in sky emissivity due to cloud cover, σ the Stefan-Boltzman constant ($5.67 \times 10^{-8} W m^{-2} K^{-4}$) and T the air temperature in Kelvin. According to Brutsaert [1975] clear-sky emissivity ε_{clear} is computed as a

[4] obtained at the 19th September 2012 via download from the following weblink: http://www.usask.ca/ip3/download/ws1/ESCIMO.spread.zip

function of air temperature T [K] and vapour pressure e [mb]:

$$\varepsilon_{clear} = C(e/T)^{1/m} \tag{2.24}$$

with the constants $C = 1.24$ and $m = 7$.
Sicart and Pomeroy [2006] state the empirical equation (2.25) to estimate F:

$$F = 1 + 0.44RH - 0.18\tau_{atm}\sigma T^4 \tag{2.25}$$

where RH is the relative air humidity and τ_{atm} the atmospheric transmissivity for shortwave radiation, which is computed as ratio of the the measured incoming shortwave radiation at the surface S and the theoretical shortwave irradiance at the top of the atmosphere S_{extra}[5]:

$$\tau_{atm} = S/S_{extra} \tag{2.26}$$

leading to the final equation (2.27) for computing incoming longwave radiation:

$$L_0 = 1.24(e/T)^{1/7}(1 + 0.44RH - 0.18S/S_{extra})\sigma T^4 \tag{2.27}$$

2.3.2.3 Adapting ESCIMO to Daily Input Data

Without any further datasets to evaluate the performance of a snow model, only the climate and snow data included in *ESCIMO.spread*, an hourly dataset from the site *Kuehroint* in the Bavarian Alps for the winter season 2004/2005, could be used to evaluate the modifications made to the adapted *ESCIMO* implementation.
Comparing *ESCIMO* runs with the original hourly data and daily averaged data, the results of model runs with averaged data showed some deviation from runs with the original data, mostly during certain days of the melting season. But considering the data availability those inaccuracies were found to be tolerable, since neither duration, nor mass balances for the accumulation and melt periods greatly differed when daily averaged data was used.
When running the model with daily time steps, the significant snowfall rate (set to 0.5 mm/hour in *ESCIMO.spread*, corresponding to 12 mm/day), which causes the snow albedo to be reset to it's maximum value, proved to be too high. Since snowfall rates

[5] which was computed according to the formulas given by Allen and Pereira [1998]

of 12 mm/day occur less seldom than snowfall rates of 0.5 mm/hour, the snow albedo declined faster, leading to higher absorption of shortwave radiation and conclusively faster ablation of the snow pack. Experimentation with different values for the significant snowfall amount showed that a significant snowfall amount of 2 mm/day for daily timesteps leads to a similar albedo development like 0.5 mm/hour for hourly time steps.

Another adaptation made to the original *ESCIMO* model structure is the consideration of tracer concentration (in this case $\delta^{18}O$) in the precipitation. The model was modified to keep track of the tracer concentration in the snowpack under the simplifying assumption of a complete mix of the tracer in precipitation and snowpack, taking their respective masses into account. This assumption is necessary because the snow model only has one layer and it might be appropriate since the snowpack's tracer concentration underlies a homogenization process, leading to high isotopic homogeneity at the time of major snowmelt, as observed by Unnikrishna et al. [2002] and Dietermann [2010].

2.3.2.4 Snow Model Output

The snow model produces several output time series. Most important is the amount of precipitation retained in the snow pack, the amount of melt water and the isotope concentration of the snow pack. Another output time series is the amount of sublimated water.

2.3.3 Precipitation and Snow Correction

The *PREVAH* precipitation data is not meant to be used directly. Within the *PREVAH*-framework ([Viviroli et al., 2009]) a precipitation and a snow correction factor are used. Both have to be calibrated for each catchment and are meant to compensate systematic errors of the input data. Thus, for this work a basic precipitation correction factor and a snow correction factor were introduced. The precipitation correction done for each single time step is described by the following equation:

$$p_C = \begin{cases} p_O \times c_R & , \ T > 0°C \\ p_O \times c_R \times c_S & , \ T \leq 0°C \end{cases} \tag{2.28}$$

where p_C is the corrected precipitation value, p_O the original precipitation value, c_R the basic precipitation correction factor and c_S the snow correction factor, which is only applied when the temperature T is equal to or less than $0°C$.

2.3.4 Modelling Chain

Compared to previous applications of the *TRANSEP* framework, this work requires a more complex scheme to obtain the final calibration results. This is due to the introduction of a snow model and the nature of the input data.

2.3.4.1 Step 1 : Semi-distributed Snow Model

Before *TRANSEP* can be used, the precipitation correction and the snow model have to be applied for each height level of a catchment, using its height level averaged climate variable values from *PREVAH*. In case an input variable is only available for the mean catchment height, its values can be corrected for each height level by applying a specified height gradient to the height difference between the current height level and the mean catchment height. This is done for the precipitation isotope concentrations, reusing the average monthly height gradients from section 2.2.5. Then the results of the snow model are aggregated, weighting the values of the different height levels by their area fraction of the whole catchment. When aggregating isotope concentrations in precipitation and melt water, not only the area fractions are taken into account, but also the amounts of water, i.e. the isotope concentrations in precipitation are weighted by the amounts of unretained precipitation and the melt water's isotope concentrations (set equal to the snow pack's isotope concentrations) are weighted by the melt water amounts. The final isotope concentrations are the mass weighted combinations of unretained precipitation and melt water concentrations. At this point, the original precipitation and precipitation isotope concentration values are replaced by snow model excess water (unretained precipitation and melt water) and the respective isotope concentrations.

2.3.4.2 Step 2: Lumped Transfer Function Model

After the semi-distributed computations of step 1 are made and all snow related issues should have been accounted for, the established lumped *TRANSEP* approach is applied.

First the parameters describing the hydraulic reaction (c, τ_w and f for the rainfall loss module and t_f, t_s and ϕ for the TPLR transfer function) are determined by calibration. Then the parameters describing the tracer signal (another TPLR transfer function with other values for t_f, t_s and ϕ) are determined, using the rainfall loss module parameters as obtained during the optimization of the hydraulic reaction. The optimizations of the 6 parameters for the hydraulic reaction and the parameters for the tracer signal are done by consecutively applying the *ACO*-algorithm (explained earlier in this chapter) two times.

The hydraulic reaction is simulated for a timespan of twenty years, where the first five years count as warm-up period and are not included in a simulation's evaluation. The tracer concentration is also simulated over a period of twenty years, with a warm-up period of fifteen years. Actually, except for the catchments *Rietholzbach Mosnang* and *Oberer Rietholzbach*, the evaluation period is even shorter, as *DroughtCH* observed runoff isotope values are only available for the last 12 to 18 months of the study. Missing tracer input concentrations were filled with day of year average values of the available input data. Wherever possible, the twenty-year simulation periods for hydraulic reaction and tracer signal should be the same. In some cases recent runoff data is missing, thus the optimization of the hydraulic parameters is done for a twenty year period which ends at the last available runoff data. The calibrated parameters for the rainfall loss module, obtained during the optimization of the hydraulic reaction, are then assumed to be the same for the later tracer simulation period.

2.3.4.3 Calibration of Precipitation and Snow Correction Factors

The precipitation and snow correction factors (see 2.3.3) have to be applied at the beginning of step 1, since they obviously have an influence on the outcome of the snow model. As the height level distributed application of the non-linear snow model takes way more time than one *TRANSEP*-simulation [6], a complete integration of the snow model into the *TRANSEP*-framework, similar to that of the rainfall loss module, seems rather impractical. Not only would the number of parameters to calibrate be increased by two, but also would the computation time of one *TRANSEP*-simulation be multiplied by a factor of at least 6 (for one height Level; for 10 height levels the factor would be

[6] Example: running the snow model takes one second for each height level while one *TRANSEP*-simulation (lumped for all height levels at once) is done within 0.2 seconds

around 50). The combination of a greater number of parameters to calibrate and longer computation times for each simulation would quickly lead to out of scale calibration times.

Therefore, the correction factors are obtained in another way: For each correction parameter a sequence of plausible values is defined. Those sequences are $[0.9, 1, 1.1, 1.2]$ for the basic precipitation correction factor c_R and $[1, 1.1, 1.2, 1.3]$ for the snow correction factor c_S. Now steps 1 and 2 are done for each possible combination of correction factors. The correction parameter combination which yields the best result at the end of step 2, i.e. lowest objective function value for the hydraulic reaction, is considered to represent the most suitable precipitation correction and its c_R and c_S values are saved. To speed this procedure up, the number of strata and maximum iterations used for the ACO(see 2.3.1.5) in step 2 can be set to low values and the determination of uncertainty (see 2.3.1.6) can be omitted. After the optimal combination of precipitation correction factors is found, a more thorough optimization with determination of uncertainties can be done.

2.4 Software

The models described in the previous section 2.3 were implemented in the open source programming language R[7]. Most of the data preparation was also done within the R environment, except for the preprocessing and analysis of geospatial data formats, which was handled by the Python environment[8] using tools provided by the Gesospatial Data Abstraction Library (GDAL[9]) and SAGA GIS[10]

[7] http://cran.r-project.org/
[8] http://www.python.org/
[9] http://www.gdal.org/
[10] http://www.saga-gis.org

Chapter 3

Results

3.1 Precipitation and runoff isotope data

The monthly integrated precipitation isotope concentrations measured at the ISOT-sites and the GNIP-site Konstanz are plotted in figure 3.1. The red line is a linear fit through all monthly values of all precipitation sites and can be understood to represent a local meteoric waterline (LMWL) described by the equation: $\delta^2 H = 7.822 \times \delta^{18} O + 5.811$. which is very close to the global meteoric water line (GMWL, depicted as grey line in figure 3.1) with the equation $\delta^2 H = 8 \times \delta^{18} O + 10$. Runoff sample isotope concentrations (blue crosses in figure 3.1) also plot on the GMWL. This suggests that fractionation through evaporation (which would alter the precipitation's isotope signature and cause some runoff samples to be plotted with a flatter slope) is not happening on a relevant scale.

3.2 Precipitation isotope data

3.2.1 Results of the interpolation procedure

3.2.1.1 Average monthly height gradients

The average monthly height-gradients ($g_{\overline{Y}M}$ from section 2.2.5) are plotted in figure 3.2. As can be seen in figure 3.2, a clear $\delta^{18} O$ height-gradient along the sites Meiringen,

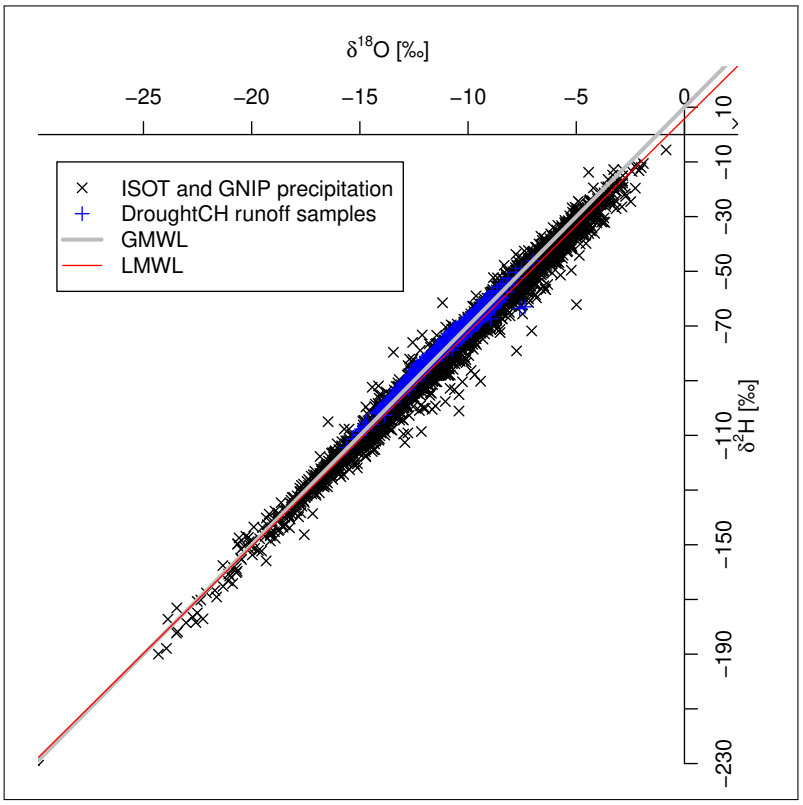

FIGURE 3.1: measured isotope concentrations in precipitation and runoff samples

Guttannen and Grimsel exists for all months' average values. The average monthly $\delta^{18}O$ height gradients range from 0.10 to 0.23‰ per 100 m and scatter around the mean value of 0.15‰ per 100 m measured by McGuire [2005] and Mueller et al. [2012](whose study investigated an area in the Ursern valley in the Swiss Alps). In general the average monthly $\delta^{18}O$ values of the other sites seem to follow that gradient, with heavier $\delta^{18}O$ enriched precipitation at lower heights. Nevertheless, most prominently during the winter months there are some outliers. Like the most south-eastern site Pontresina, which has by far the lightest values of all sites throughout December to March, even though it lies 200 m below the highest site (Grimsel). On the other side, there is the western site La Brevine, whose average november to march values are as heavy as the values of sites lying 500 lower. Besides that, it has to be noted that the value ranges of each site's monthly values are rather big and that values of specific months (instead of averaged values from 15 years) rarely are aligned along a distinguishable height-gradient.

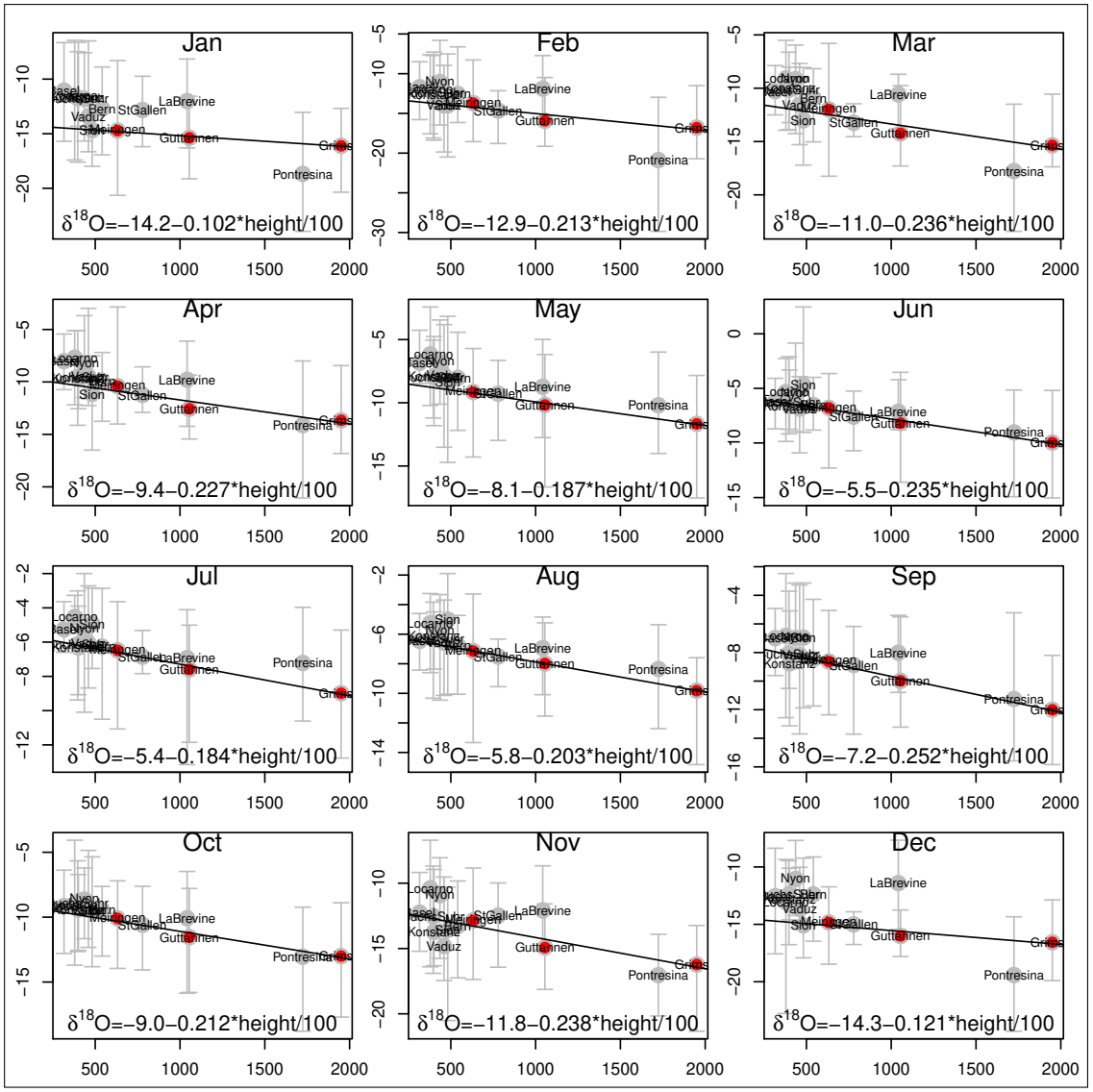

FIGURE 3.2: Average monthly height-gradients (black lines) along the three ISOT-sites Meiringen, Guttannen and Grimsel (red points); other sites' average monthly values (grey points) and the ranges of all monthly values(grey bars); x-axis: height above sealevel [m], y-axis: $\delta^{18}O$ [‰]

3.2.1.2 Average spatial $\delta^{18}O$ pattern

The interpolation of average monthly height-gradient normalized precipitation $\delta^{18}O$ values, as decribed in section 2.2.5, lead to the monthly maps in figure 3.3, which shows the spatially interpolated theoretical average monthly sea level $\delta^{18}O$ values in precipitation, based on measured $\delta^{18}O$ values of the thirteen ISOT-sites and the GNIP-site Konstanz. The monthly maps show a seasonal cycle of sea-level $\delta^{18}O$ values in precipitation for the entire area of Switzerland with lighter values for the winter season and heavier ones during the summer months. In the winter months December, January and February

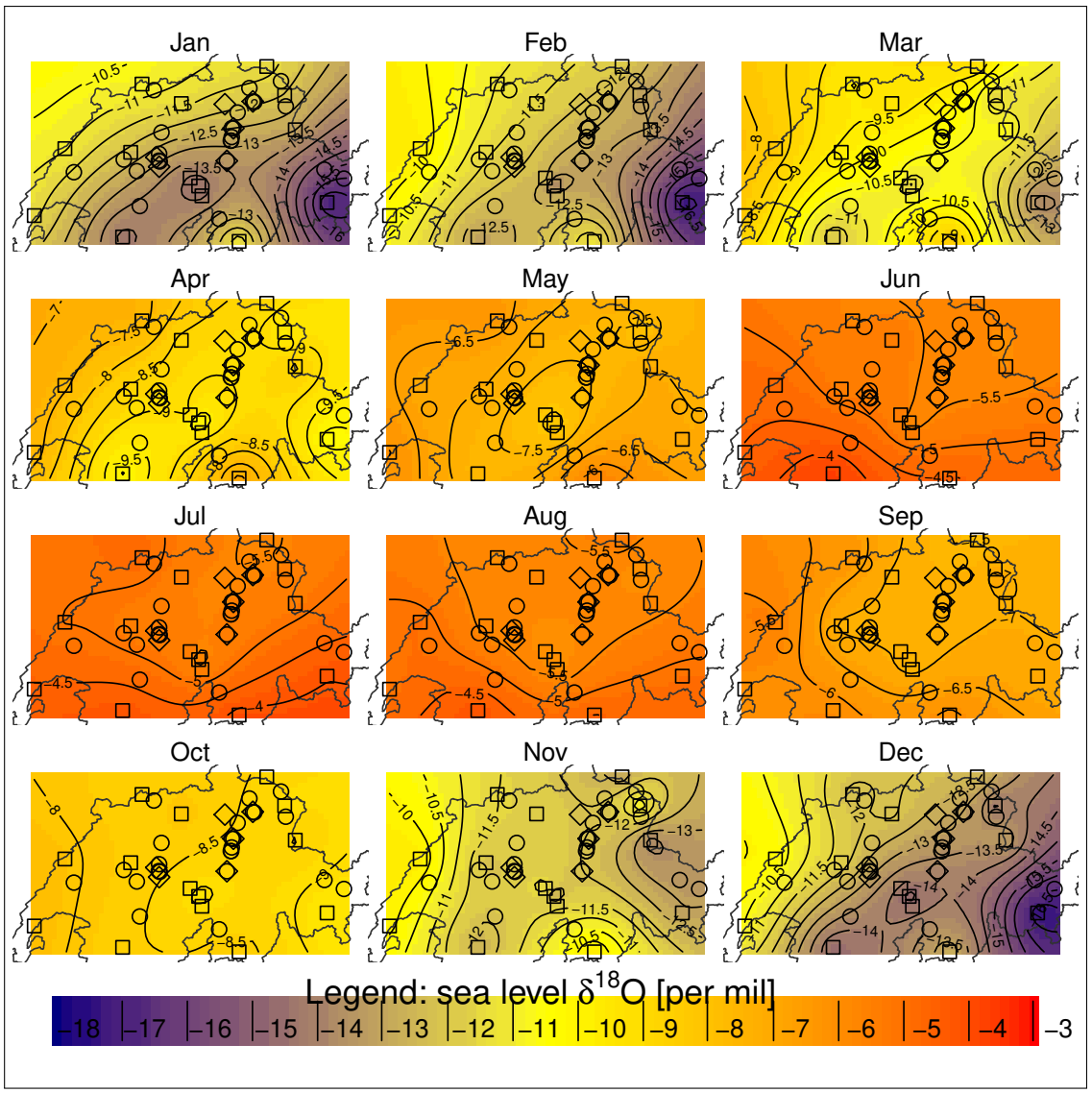

FIGURE 3.3: Monthly maps of interpolated sea level precipitation $\delta^{18}O$ values; boxes: ISOT and GNIP precipitation measurements sites, circles: Drought-CH runoff sample sites, diamonds: Drought-CH precipitation sample sites and Messstelle Buel

there is a clearly negative $\delta^{18}O$ trend from north-west to south-west, with a maximum difference of around 6‰. This trend decreases throughout the spring, leading to a rather weak positive $\delta^{18}O$ trend from north to south during the months of June to August, with a maximum of less than of 2‰. From September to November the trend is negative from west to east and particularly weak in October with a maximum difference around 1‰.

3.2.2 Evaluation of predicted precipitation $\delta^{18}O$

Available data to evaluate the interpolation based $\delta^{18}O$-predictions was sparse. Within the Drought-CH project precipitation samples to determine $\delta^{18}O$ were taken at five sites, with the longest data record covering the year 2011 and the shortest data record ranging from August to end of September 2011. A longer data record was available for the site *Messstelle Buel* (maintained by the IAC of ETH-Zurich), which lies within the research catchment Rietholzbach. Figure 3.4 shows a comparison of the observed (red lines) and predicted values (black lines, obtained by the interpolation procedure described in 2.2.5). Except for the site Aeschau, whose assumed elevation is not confirmed, the observed and predicted values seem to be in good agreement. However, the differing sampling intervals - predictions are based on monthly samples, observed samples were collected for varying intervals ranging from single weeks to two months - and unknown precipitation amounts at all sampling sites do not allow for a quantitative evaluation of the prediction.

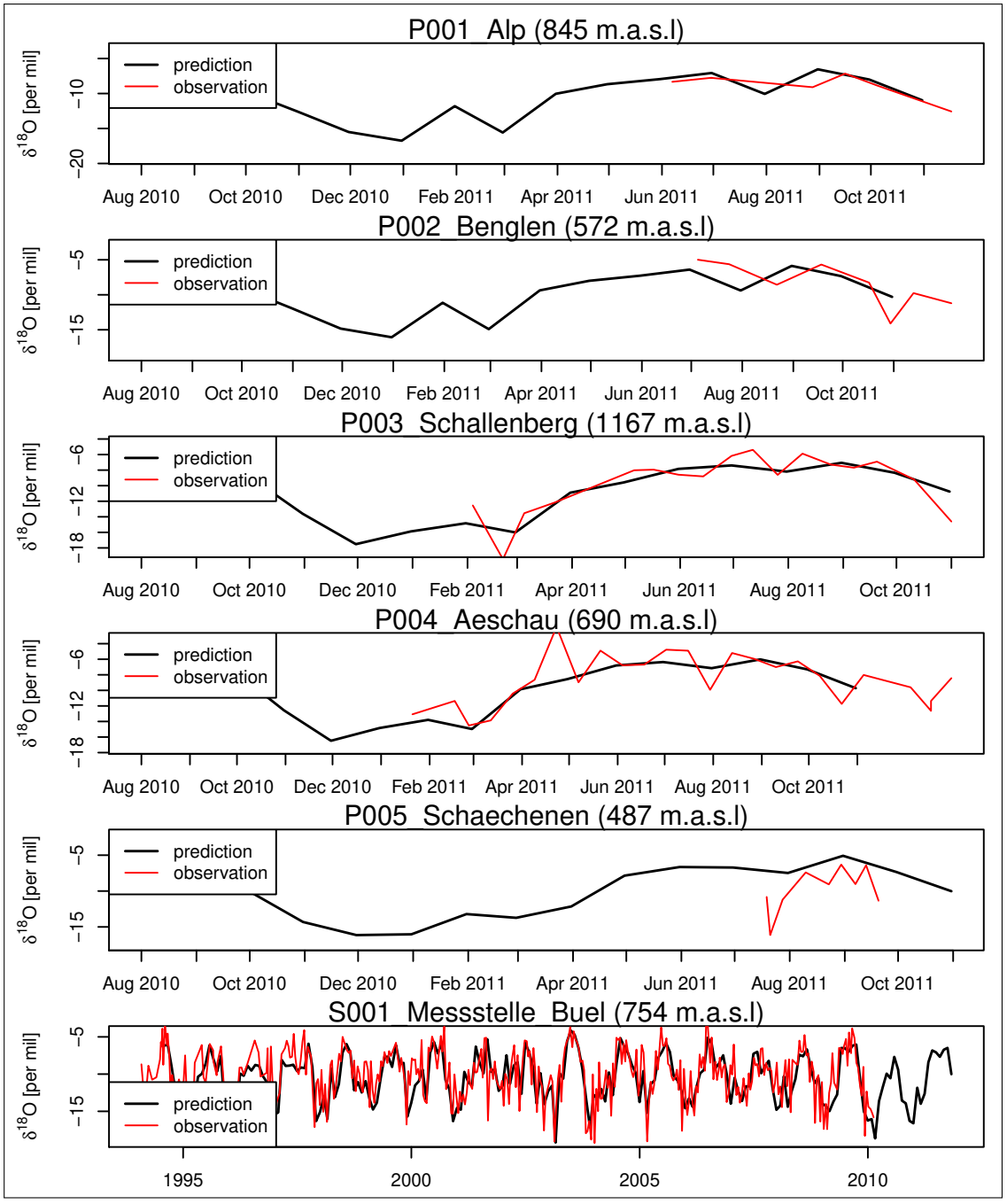

FIGURE 3.4: Comparison between predicted and measured $\delta^{18}O$ values

3.3 Simulation Results

3.3.1 Snow model

As no snow data was available to evaluate the performance of the uncalibrated snow model, the best way to evaluate the simulation results, is to look at the simulated

snow water equivalents (SWE) and the observed runoff values. In general, the snow model managed to simulate snow accumulation, marked by receding runoff and increasing SWE, and melt periods, marked by decreasing SWE and high runoff, quite accurately. As excepted from the runoff regime classification(see 2.1.0.1), the simulated snow water equivalents and snow retained precipitation amounts were highest for the catchments with the highest mean elevations (see top of figure 3.5 for the highest catchment *Dischmabach*) and decreased with decreasing catchment elevation. For the lowest catchments (e.g. *Ergolz* at the bottom of figure 3.5), simulated maximum SWE values were smaller by one order of magnitude and the accumulation periods were often interrupted by melt events before the end of winter.

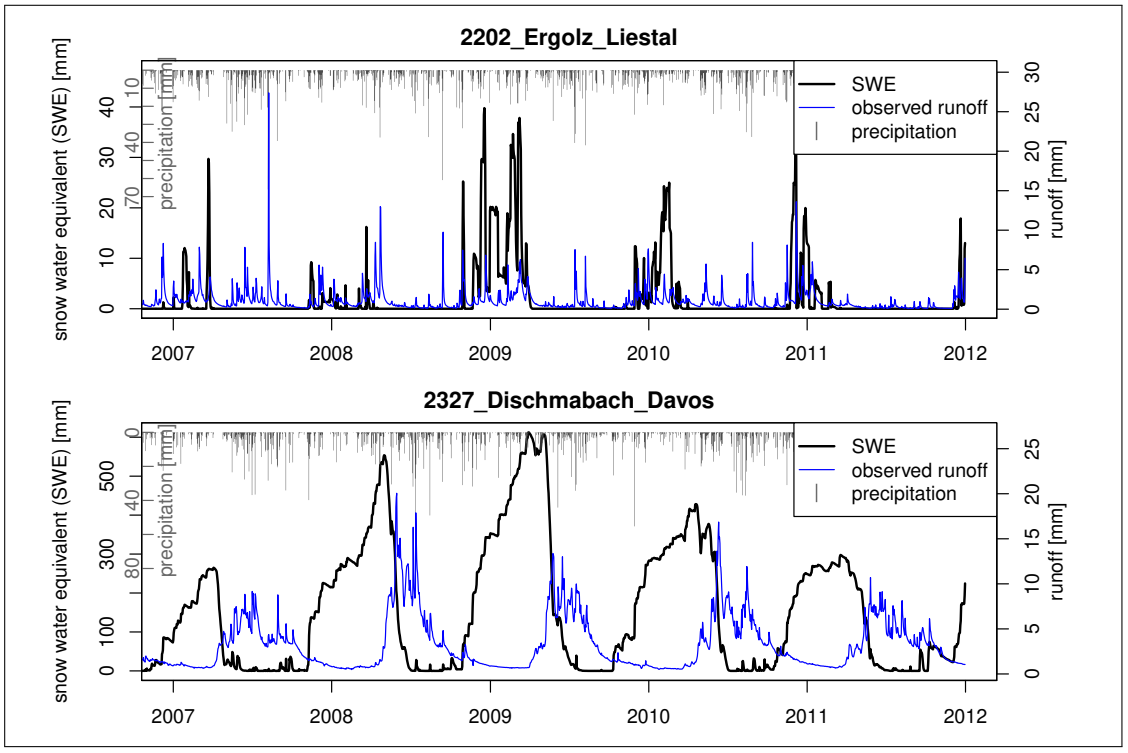

FIGURE 3.5: Simulated snow water equivalents and observed runoff for the catchments Dischmabach-Davos and Ergolz-Liestal for the last five years of the simulation

3.3.2 Rainfall-runoff model

3.3.2.1 Simulated yearly evapotransiration

Menzel [1999] stated average yearly evapotranspiration sums of 560 mm for catchments around 700 m and around 230 mm for catchments at 3000 m. The simulated evpaotransipration sums loosely align along this trend, but except for the catchment *Aabach-Moencahltorf*, which incorporates a lake, the magnitude of deviations can hardly be explained by differences in vegetation cover or other microclimatic features.

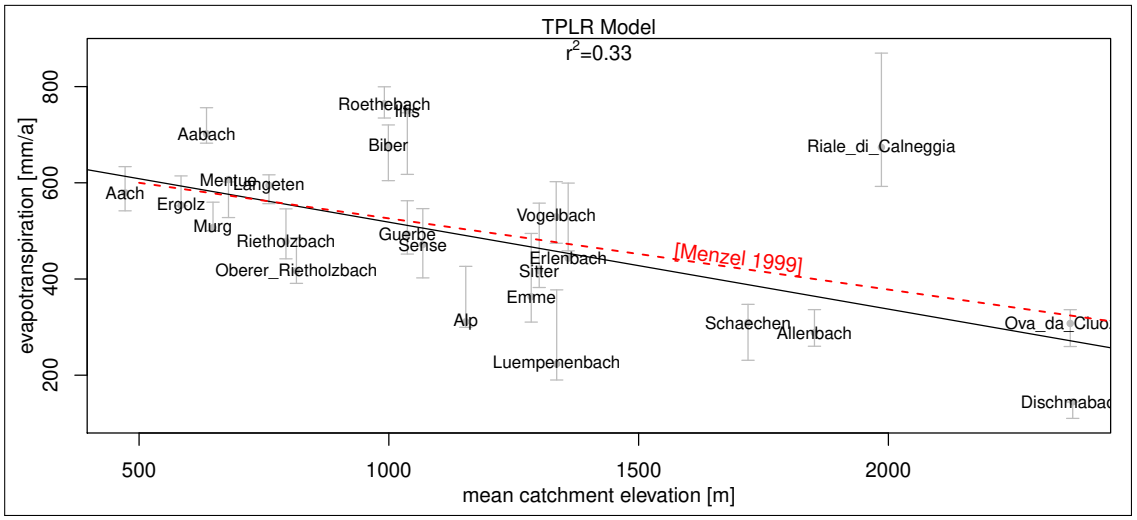

FIGURE 3.6: Yearly simulated evapotranspiration sums plotted against catchment elevations. Grey bars indicate values of 20 near to best simulations. The black line indicates the trend of all the simulated values and the red line indicates the trend statet by **??**

Acoording to the *Swiss Federal Institute for Forest, Snow and Landscape Research* (WSL), average yearly evapotranspiration sums for the catchments *Vogelbach*, *Luempenenbach* and *Erlenbach* amount to 558, 425 and 512 mm, respectively[1]. The simulated yearly evapotransiration sums for the catchments Vogelbach and Erlenbach lay between 460 and 600 mm and therefore included the values stated by the WSL. The best simulations for the catchment Luempenenbach implied values between 190 and 380 mm which is clearly below the value stated by the WSL. Also very striking is the high average yearly evapotranspiration sum for the catchment *Riale de Calneggia*. The calibrated parameter sets of simulations with the highest objective function values suggest a yearly sum

[1]Data obtained from the WSL website: http://www.wsl.ch/fe/gebirgshydrologie/testgebiet_alptal [visited 12.12.2012]

between 600 and 850 mm - for a catchment with a mean elevation around 2000 m and an annual mean temperature of 3° Celsius. The values for the catchments *Roethebach*, *Ilfis* and *Biber* also lay far above the expected values. For the catchment *Dischmabach*, the calibration lead to an average yearly evapotranspiration sum around 130 mm, which clearly lies below the value stated by Zappa and Gurtz [2001], who computed a value around 220 mm/a.

3.3.2.2 Simulated runoff

The calibration of the hydraulic model, a combination of the non-linear rainfall loss module after Jakeman and Hornberger [1993] and the TPLR proved to yield good solutions, i.e. NSE and logNSE values above 0.6 for almost all catchments (see table(A.1) in the appendix).

The value ranges of the three rainfall loss module parameters (see figure(A.1) in the appendix) could hardly be identified. For most of the catchments, optimal solutions could be found across a good part of the initial parameter ranges. In a few cases a part of the optimal solutions was found outside of the initial parameter bounds.

Parameter identifiability was a little better for the TPLR runoff model (see figure(A.1) in the appendix). The catchment with the shortest simulated mean reaction time was *Ergolz-Liestal* with mean reaction time estimates ranging from 10 to 30 days (median: 18 days). The longest mean reaction time, with estimates ranging from 96 to 156 days (median: 126), was simulated for the catchment *Langeten-Huttwil*. During the calibration, the upper initial bound for the TPLR-parameter τ_s (mean reaction time of the slow reservoir) was transgressed for over half of the catchments, indicating that the initial upper bound for τ_s of 150 might have been too low. A striking result is that the simulations with the highest NSE and logNSE values have been made for catchments with nival runoff regimes (e.g.: *Dischmabach*, *Ova da Cluozza* and *Schaechen*).

3.3.3 Tracer models

3.3.3.1 Exponential tracer model

The results of the calibration of exponential tracer models are shown in table(3.1). The only parameter of the exponential model is the MTT. Therefore it could be determined

without any ambiguity. The first striking thing to see, is that all simulations had a negative bias, i.e. the simulated runoff $\delta 18O$ values lie systematically below the observed values. An attempt to calibrate the models directly with the NSE as objective function, without the prior elimination of the bias, did not succeed. The most extreme simulation bias values (-2.1 and -3) belong to the catchments *Ova da Cluozza* and *Riale de Calneggia*, respectively. Incidentally, these two catchments belonged to the only six catchments for which a simulation with a median normalized NSE above 0.4 could be achieved. The MTTs for those seven catchments ranged from 0.4 to 2 years. The longest MTTs with about 20 years, were estimated for the catchment *Rietholzbach Mosnang* and its subcatchment *Oberer Rietholzbach*.

Following the remarks of McGuire and McDonnell [2006], MTTs wich are longer than 1/4 of the simulation period have to be considered as more uncertain, since a good portion of the observed tracer concentration in runoff originates from tracer inputs before the start of the simulation period.

3.3.3.2 Gamma distribution tracer model

Table 3.2 shows the results for the calibrated gamma distribution tracer models. The prediction bias for this model type is similar to the bias of the exponential models. A median normalized NSE above 0.4 could be reached for fourteen catchments. On the other hand, the MTT estimates for seven catchments were unexpectedly high, with durations of 30 years and more. Except for the catchment *Aabach*, where the MTT was estimated to be around 13 years, all other acceptable simulations belong to catchments whith shorter MTT estimates between 0.7 and 2.5 years. The uncertainty ranges of the calibrated model parameters are shown in figure(3.7). Generally all model parameters were identifiable. With more calibration effort, i.e. running the ACO-algorithm with more strata and a higher iteration limit, the remaining uncertainties could have been eliminated.

TABLE 3.1: Calibration results for the exponential tracer model. Median normalized NSE values above 0.4 are bold. Bias Values below -1 are in italics. Mean transit times above five years (1/4 of the 20 year simulation period) are marked with an asterisk

Catchment	medianNormalizedNSE	bias [$\delta^{18}O$]	MTT [a]
Oberer_Rietholzbach	0.0249	-0.67	21*
Vogelbach	**0.5292**	-0.47	0.4
Luempenenbach	**0.4741**	-0.35	0.5
Roethebach	-0.0134	-0.60	6.7*
Erlenbach	0.697	-0.78	0.2
Aabach	0.2048	*-1.53*	1.4
Sitter	**0.781**	*-1.35*	0.8
Murg	0.0569	*-1.41*	4.7
Sense	0.3862	*-1.05*	1.5
Ergolz	0.0463	*-1.98*	2.2
Allenbach	0.3185	*-1.46*	1.6
Aach	0.0031	*-1.22*	9.7*
Ova_da_Cluozza	**0.4529**	*-2.09*	1.0
Dischmabach	0.3894	-0.79	2.3
Langeten	0.039	-0.77	9.2*
Riale_di_Calneggia	**0.7531**	*-3.02*	0.6
Mentue	0.1142	*-1.88*	1.2
Emme	0.2691	*-1.44*	1.1
Rietholzbach	-0.0019	-0.79	21.1*
Guerbe	**0.6617**	*-1.10*	1.4
Schaechen	**0.7611**	-0.40	2.0
Ilfis	0.1285	-0.72	3.8
Biber	0.2171	-0.59	0.8
Alp	0.3144	-0.87	0.7

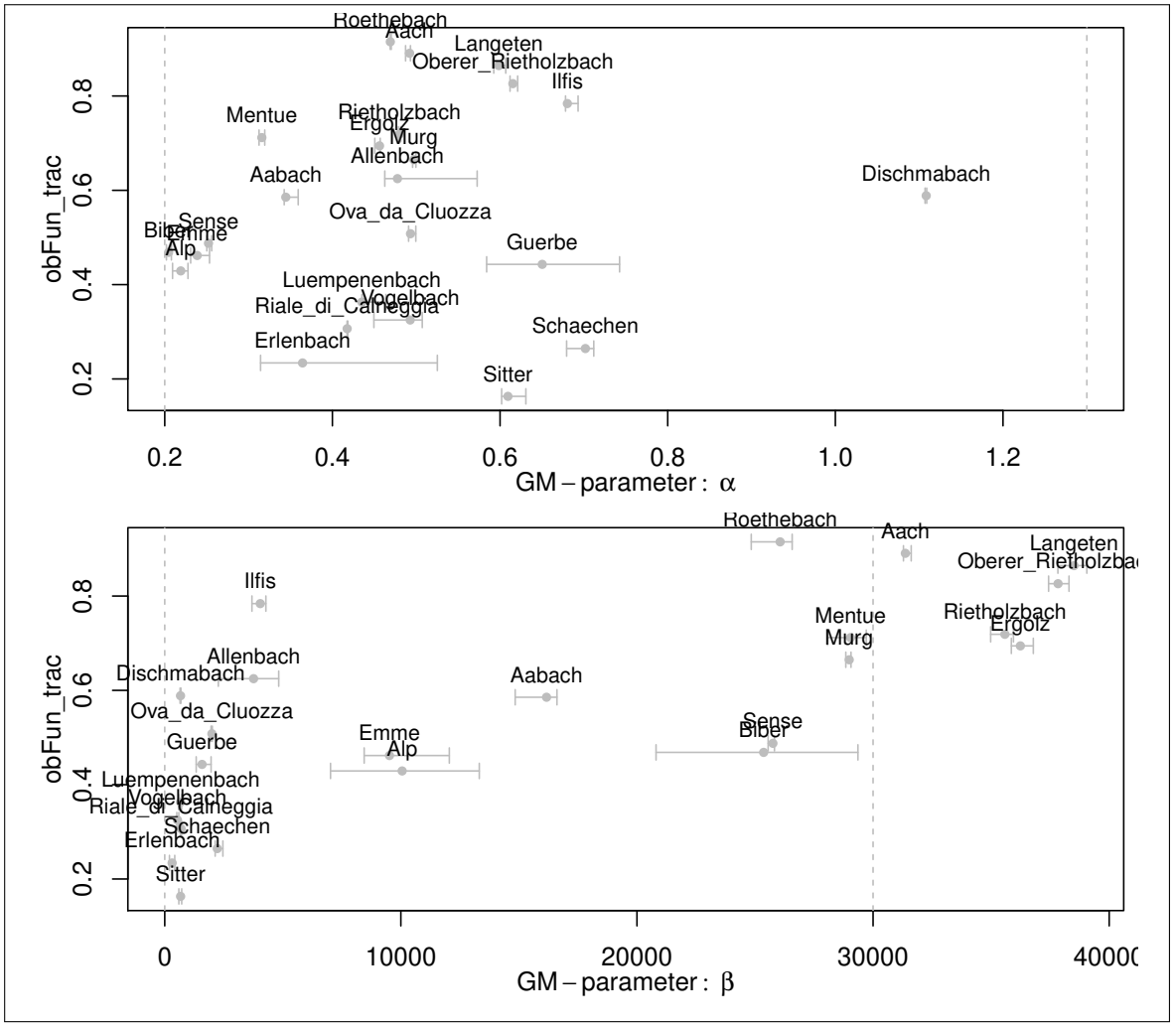

FIGURE 3.7: Calibrated parameter values for the gamma distribution tracer models. The grey dashed lines indicate the initial parameter bounds. Grey bars indicate the parameter values for 21 near to best simulations

TABLE 3.2: Calibration results for the gamma distribution tracer model. MTT ranges are based on 21 equally optimal simulations, the stated gamma distribution parameters belong to the simulation with the median MTT

Catchment	medianNormalizedNSE	bias	MTT [a]			gamma distribution	
			median	min	max	α	β [d]
Oberer_Rietholzbach	0.17	-0.69	63.8*	63*	64.9*	0.62	37826
Vogelbach	**0.68**	-0.62	0.7	0.7	0.8	0.48	548
Luempenenbach	**0.64**	-0.58	0.8	0.7	0.9	0.45	655
Roethebach	0.09	-0.65	33.5*	32*	34.2*	0.47	26063
Erlenbach	**0.77**	-0.83	0.3	0.2	0.4	0.37	297
Aabach	**0.41**	*-1.30*	15.3*	14.3*	15.9*	0.35	15785
Sitter	**0.84**	*-1.16*	1.1	1.0	1.2	0.61	670
Murg	0.34	*-1.32*	39.5*	39.3*	39.8*	0.50	28969
Sense	**0.51**	-0.78	17.8*	17.5*	18.1*	0.25	25745
Ergolz	0.31	*-1.69*	45.3*	44.6*	45.9*	0.45	36392
Allenbach	0.38	*-1.40*	4.9	3.2	6.3*	0.51	3378
Aach	0.11	*-1.37*	42.3*	41.9*	42.6*	0.49	31499
Ova_da_Cluozza	**0.49**	*-1.71*	2.7	2.6	2.8	0.50	1987
Dischmabach	**0.41**	-0.93	2.0	2.0	2.1	1.11	668
Langeten	0.14	-0.84	63.2*	62.2*	64.7*	0.60	38480
Riale_di_Calneggia	**0.69**	*-2.94*	0.8	0.8	0.8	0.42	692
Mentue	0.29	-0.97	25.1*	24.4*	25.8*	0.32	29010
Emme	**0.54**	*-1.24*	6.2*	5.5*	7.7*	0.24	9518
Rietholzbach	0.28	-0.90	46.8*	46*	47.2*	0.48	35592
Guerbe	**0.56**	-0.96	2.8	2.4	3.2	0.64	1597
Schaechen	**0.74**	-0.46	4.3	4.1	4.6	0.69	2248
Ilfis	0.22	-0.61	7.5*	7*	8*	0.69	4044
Biber	**0.53**	-0.46	14.2*	11.7*	16.2*	0.20	25365
Alp	**0.57**	-0.73	6*	4.4	7.6*	0.22	10059

3.3.3.3 Two parallel linear reservoir tracer model

Table 3.3 shows the calibration results of for the TPLR tracer models. Like for the previous models, all simulations have a negative prediction bias. With the TPLR tracer model, 16 of the 24 catchments reach a median normalized NSE above 0.4. The MTTs of the seven best simulated catchments (with a median normalized NSE above 0.6) were estimated to values of 4.3 years and shorter, while except for the catchment *Ilfis-Langnau* with an estimated MTT around 7.1 years, all catchments with median normalized NSE values below 0.4 have estimated MTTs over ten years.

Figure 3.8 shows the calibrated parameters for the TPLR tracer model. The initial upper bound for the mean transit time of the slow reservoir τ_s has been transgressed during the calibration of several catchments, while these catchments' fraction of the fast reservoir Φ got close to 0. This lead to very high mean transit times for these catchments. For another group of catchments, the τ_s values got very close to the initial lower bound, while the Φ values remained rather high. This means, that those catchments have smaller mean transit times, as a bigger fraction of the water goes through their fast reservoirs and the mean transit times of the slow reservoir are relatively small. For a third group of catchments, some of them with the best objective function values (e.g. *Sitter*, *Schaechen* and *Riale de Calneggia*), the parameters were not identifiable, as indicated by the wide uncertainty bars in figure(3.8).

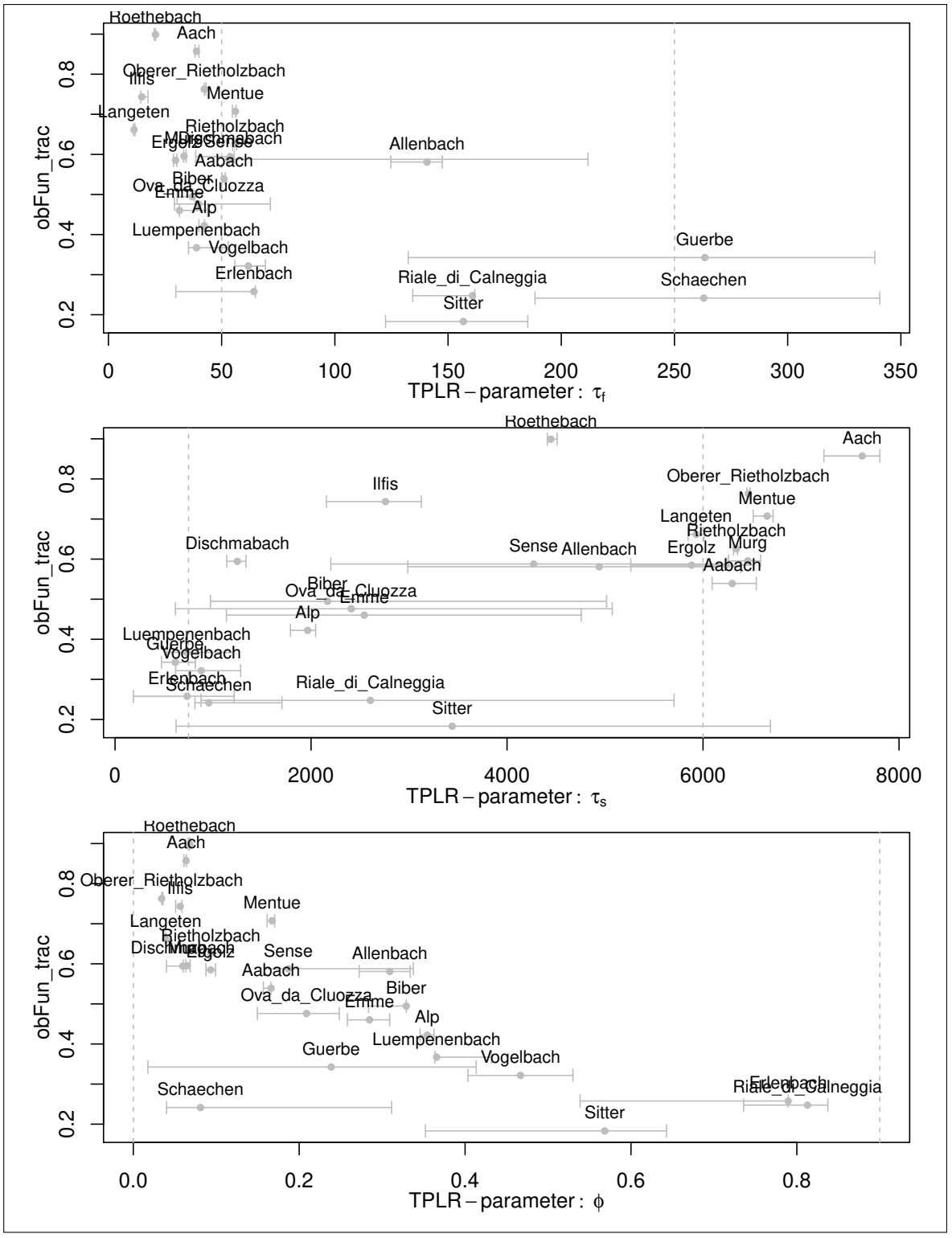

FIGURE 3.8: Calibrated parameter values for the TPLR tracer models. The grey dashed lines indicate the initial parameter bounds. Grey bars indicate the parameter values for 21 near to best simulations

TABLE 3.3: Calibration results for the two parallel reservoir tracer model. MTT ranges are based on 21 equally optimal simulations, the stated gamma distribution parameters belong to the simulation with the median MTT.

Catchment	medianNormalizedNSE	bias	MTT [a]			Two parallel linear reservoirs		
			median	min	max	τ_f [d]	τ_s [a]	Φ
Oberer_Rietholzbach	0.24	-0.69	17.1*	17.1*	17.1*	42.7	17.7	0.035
Vogelbach	**0.68**	-0.71	1.4	0.9	1.9	61.8	2.4	0.468
Luempenenbach	**0.63**	-0.66	1.3	0.9	2.0	44.8	2.0	0.399
Roethebach	0.10	-0.60	11.4*	11.3*	11.5*	20.5	12.2	0.067
Erlenbach	**0.74**	*-1.01*	0.6	0.3	1.4	42.2	1.9	0.621
Aabach	**0.46**	*-1.14*	14.4*	14*	15*	50.8	17.2	0.163
Sitter	**0.82**	*-1.22*	4.3	1.2	8*	173.2	9.4	0.571
Murg	0.40	*-1.19*	16.5*	16*	16.9*	33.6	17.7	0.066
Sense	**0.41**	-0.65	9.5*	4.3	13*	163.6	12.4	0.274
Ergolz	**0.42**	*-1.59*	14.6*	13*	16.2*	29.4	16.1	0.095
Allenbach	**0.42**	*-1.31*	9.5*	5.8*	12.5*	134.7	13.5	0.301
Aach	0.14	*-1.20*	19.6*	18.6*	20.1*	39.0	20.9	0.063
Ova_da_Cluozza	**0.52**	*-1.71*	5.2*	1.4	11.6*	49.8	6.5	0.194
Dischmabach	**0.41**	-0.71	3.2	3.0	3.5	49.9	3.4	0.050
Langeten	0.34	-0.72	15.6*	15.4*	15.8*	11.4	16.2	0.039
Riale_di_Calneggia	**0.75**	*-3.01*	1.7	0.9	3.7	153.2	6.7	0.791
Mentue	0.29	-0.60	15.2*	14.9*	15.4*	55.6	18.2	0.167
Emme	**0.54**	*-1.26*	5.0	2.3	9.6*	37.5	7.0	0.277
Rietholzbach	0.37	-0.87	15.8*	15.7*	15.8*	55.7	17.4	0.093
Guerbe	**0.66**	*-1.08*	1.5	1.3	1.7	284.5	1.6	0.226
Schaechen	**0.76**	-0.42	2.5	2.1	3.6	319.6	2.7	0.160
Ilfis	0.26	-0.60	7.1*	5.6*	8.1*	14.6	7.6	0.055
Biber	**0.51**	-0.44	4.0	1.9	9.9*	35.0	5.9	0.309
Alp	**0.58**	-0.63	3.5	3.2	3.7	41.3	5.4	0.355

3.3.3.4 Model comparison

Comparison of estimated mean transit times Figure 3.9 shows a comparison of all MTT estimates for all three model types. The catchments were ordered after the MTT estimates of the TPLR models. It can be noted, that there is never a close agreement of all three model types. The MTT estimates for TPLR and the gamma distribution model match for the catchments *Aabach* (around 15 years), *Ilfis* (around seven years) and *Emme* (between five and six years). TPLR and exponential model agree for *Guerbe* (around 4.5 years), *Schaechen* (around 2.2 years) and *Oberer Rietholzbach* (between 17 and 20 years). Exponential and gamma distribution model agree for *Dischma* (around 2 years) and *Sitter* (around one year).

In general, when just the ranks of the MTTs are compared, there are no big differences bewteen the three model types: the catchments with the shortest MTTs for one model type are the catchments with the shortest MTT estimates for the other model types. Compared to the TPLR model, the gamma distribution model estimates smaller values for catchments with small MTTs and much bigger values for catchments with long MTTs, whereas the exponential model tends to estimate all MTTs shorter than the TPLR model.

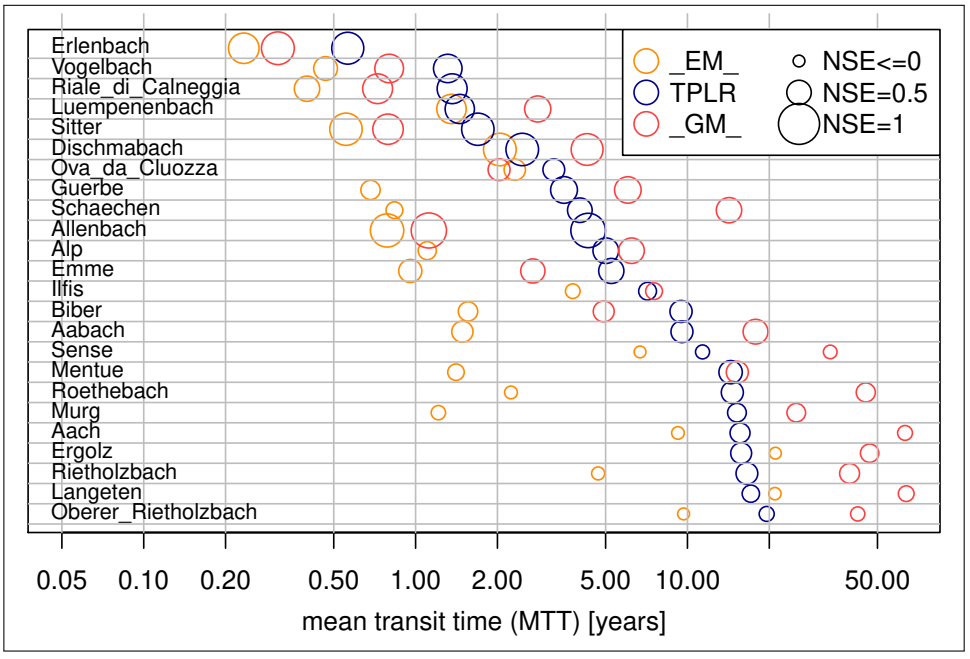

FIGURE 3.9: Comparison of MTT estimates of all three model types for all catchments. NSE in the figure actually stands for the median normalized NSE. _EM_ is the exponential model, _GM_ the gamma distribution.

Comparison of tracer concentration curves A comparison of the simulated tracer concentrations (see figure3.10) reveals some issues which would remain unnoticed if only objective functions and calibrated parameter values and MTTs were considered.

Similar time series despite clearly different MTT For the catchment *Sitter Appenzell*, the tracer simulations of all three models produced very similar tracer concentration time series, which, prediction bias aside, are in good agreement with the observed values . Whilst the calibrated parameters of the exponential model and the gamma distribution model lead to MTTs of around 1 year, the calibrated parameters of the TPLR model imply a MTT of 4.3 years (while equally good parameter sets for simulations with MTTs between 1.2 and 8 years have been found).

Temporal variability of prediction goodness Longer $\delta^{18}O$ runoff observation time series, covering several years, were only available for the catchments *Rietholzbach* and *Oberer Rietholzbach* and the calibrations for the catchment *Oberer Rietholzbach* yielded rather bad objective function values. The tracer concentrations for the catchment *Rietholzbach* (see middle of figure(3.10) could more or less successfully be predicted by the TPLR and the gamma distribution models. It can be noted, that the model fits were rather good between 2008 and the beginning of 2011, whereas the predictions clearly deviated from the observed tracer concentrations during the years 2007 and 2011. Hrachowitz et al. [2010] showed that the gamma function's parameter β can be considered as variable and strongly related to the precipitation amount above a certain threshold. A similar non-stationary behaviour of the parameters of the TPLR can be imagined. However, since no further longer data records were available, it was not possible to investigate this issue any further.

Temporary model agreement - despite bigger differences The plotted simulation results for the catchment *Ova da Cluozza* (bottom of figure(3.10) show that there can be a temporary overlap (from mid of 2009 to end of 2011) of different transfer function models, leading to similarly optimal predictions of the observed values, even if the models actually do not behave the same (from 20007 to mid of 2009). Even though the models have clearly differing bias values, the removal of the bias before the evaluation of the objective function leads to very similar objective function values.

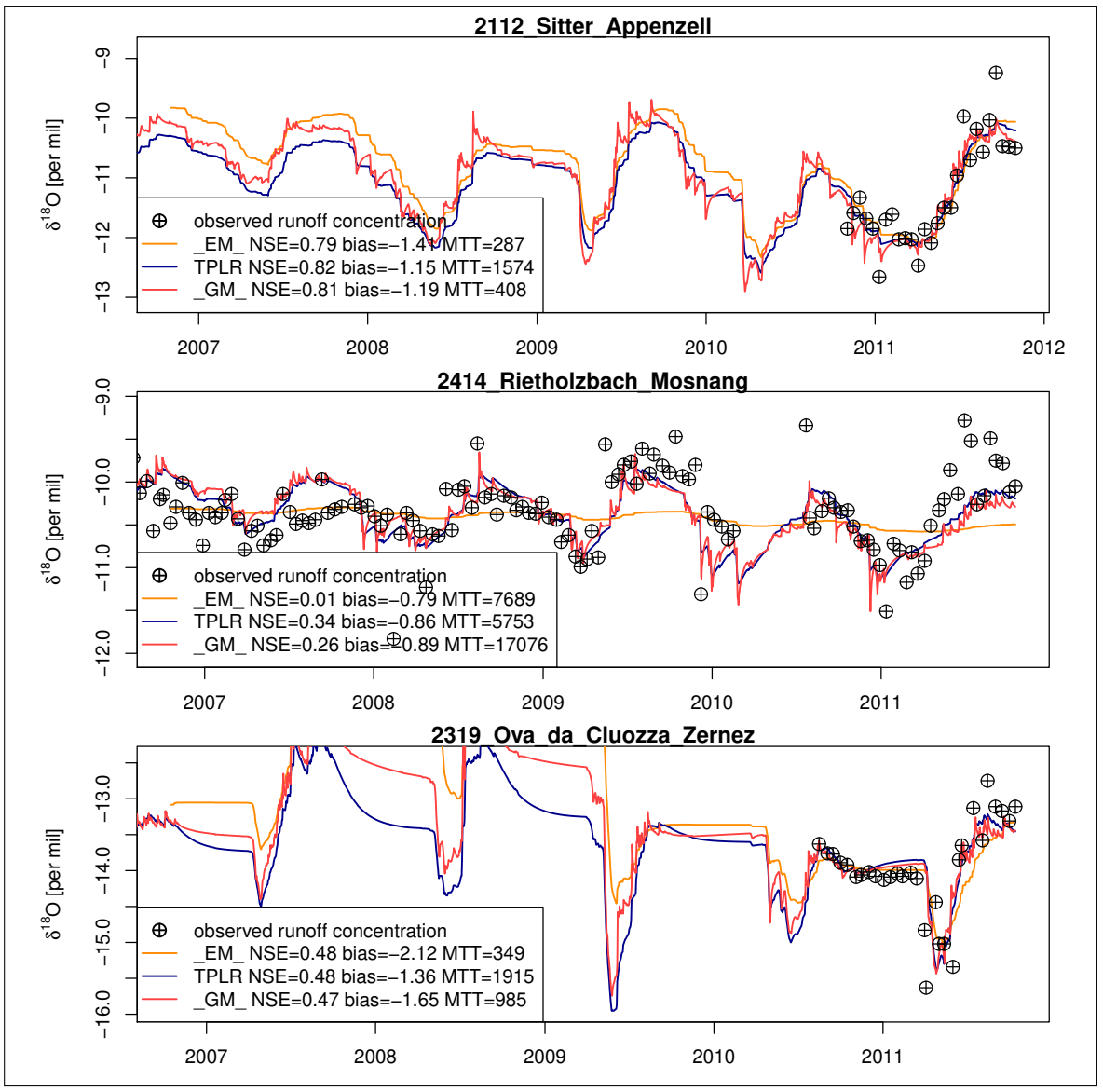

FIGURE 3.10: Simulated and observed tracer time series. The curves are plotted with an offset to compensate the prediction bias, stated in the legend. _EM_ is the exponential model and _GM_ the gamma distribution model. NSE is actually the median normalized NSE

3.3.3.5 Catchment characteristics and MTT

The correlations of estimated MTTs with median flowpath lengths and median catchment slopes have been tested. However, none of those topographic characteristics showed a higher correlation with the estimated MTTs than the mean catchment elevations. As these catchment characteristics are closely correlated with the mean catchment elevations, it can be assumed that, for the considered set of catchments as a whole, the explanatory power of these catchment characteristics is rather small.

Figure(3.11) shows the estimated MTTs plotted against the mean catchment elevations. Because of the comparatively high MTT estimates for the catchments *Rietholzbach Mosnang* and *Oberer Rietholzbach* - both have MTTs of over 20 years, while none of the other catchments' MTT exceeds 10 years - the coefficient of determination for the exponential model is very low. If these two catchments were removed, the resulting coefficient of determination would be close to the coefficient of determination obtained for the other two models. However, even for the gamma distribution model and the TPLR model the coefficients of determination remain rather small with values of 0.44 and 0.46, respectively.

Roughly speaking, the catchments can be parted into two fractions which have no significant height gradient: catchments above 1000 m, with MTTs of less than 10 years and catchments below 1000 m with MTTs above 10 years. Whereas the MTTs of the lower catchments which were estimated with the gamma model easily exceed 20 years and reach up to 60 years, the longest MTTs estimated with the TPLR model range from 10 to 20 years. The exponential model's MTT estimates remain significantly shorter for most of the lower catchments, but the efficiencies for those simulations were the worst.

Within the higher elevated fraction of the catchments, ranging from 1000 to 2500 m, the catchments with the lowest MTT estimates are *Erlenbach*, *Vogelbach*, *Luempenenbach* (all three located in the Alptal around 1500 m) and *Riale de Calneggia* (around 2000 m). Catchments with elevations below, between and above those catchments have higher MTTs.

It has to be noted, that all the catchments of the lower fraction with high MTTs are located on the Swiss plateau, where the underlying geology mostly consists of heavy layers of fissured sedimentary rock, the molasse, whilst the higher located catchments mainly are located on solid bedrock and have relatively undeveloped and thin soil layers.

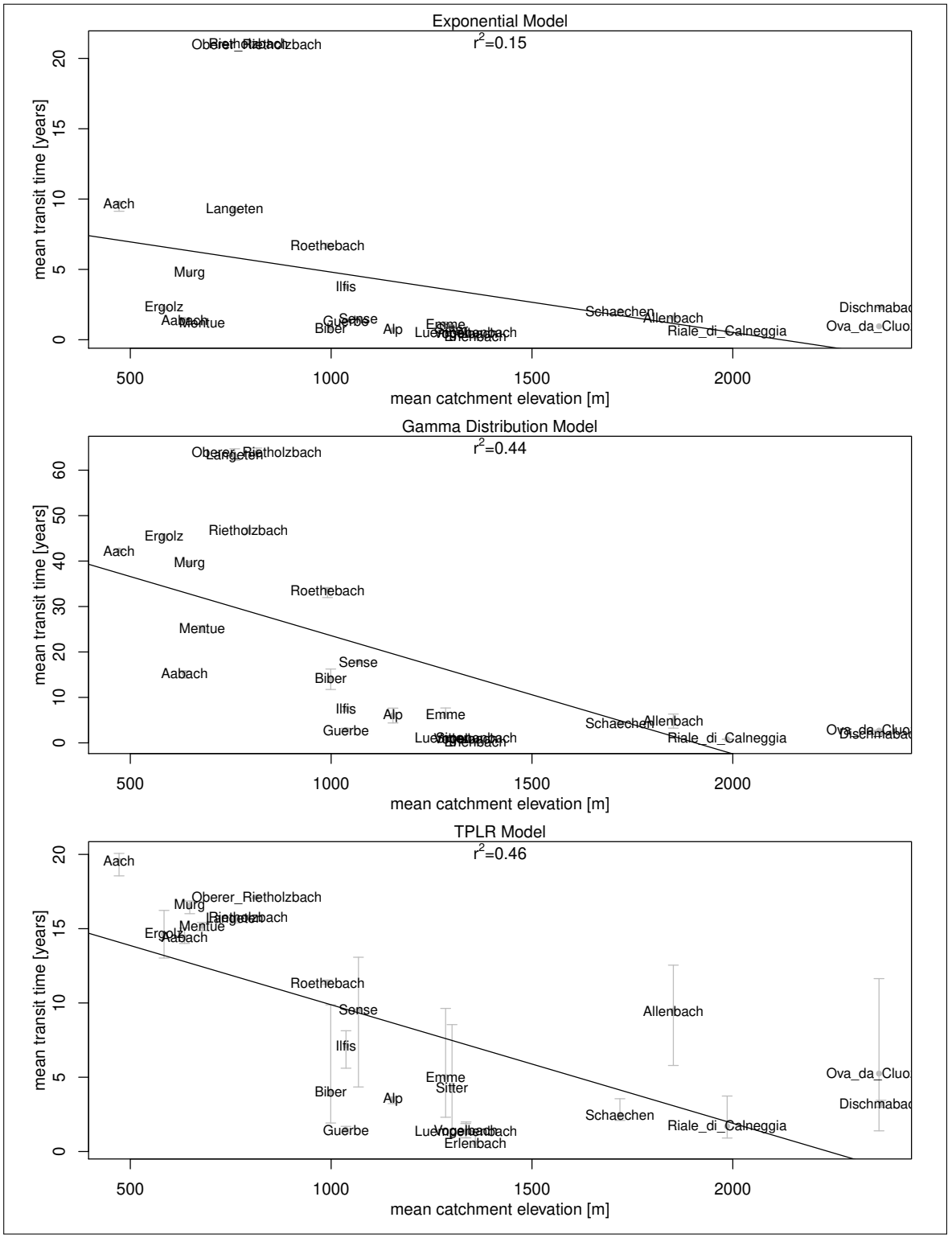

FIGURE 3.11: MTTs of each model type plotted against elevation. Grey bars indicate the range of MTT values for 21 near to best simulations

3.3.3.6 Estimation of total catchment water storage

Figure(3.12) shows the estimated values for total catchment storages and dynamic catchments storages based on the MTT estimates (from TPLR tracer concentration models) and MRT etsimates (from TPLR runoff models), respectively. Since total and dynamic catchment storages were computed as products of the mean water flux rates with MTT and MRT, respectively, and mean runoff rates do not differ in orders of magnitude, the resulting storage estimates' distributions closely resemble the MTT, respectively MRT distributions. The TPLR tracer model based total storage estimates of catchments with comparatively good objective function values for the tracer model reach up to 10000 mm (*Aabach*) but with the exception of the catchment *Sitter*(which has a very high uncertainty and could as well have a much lower value) the catchments with the highest objective function values have the smallest total storage estimates. Generally, there seems to be no relation between total and dynamic catchment storages. The fact, that the dynamic storage for the catchment *Erlenbach* is estimated to be higher than its total storage volume, which is impossible, illustrates how uncertain the estimates are. Total storage estimates for behavioral exponential models ranged from 392 mm for *Erlenbach* to 3000 mm for *Dischmabach*. The smallest estimated total storage values for the gamma distribution also belonged to *Erlenbach* with a uncertainty range between 380 and 610 mm. Amongst the behavorial gamma distribution models, the catchment *Alp* had the highest storage values within an uncertainty range from 13000 to 18000 mm.

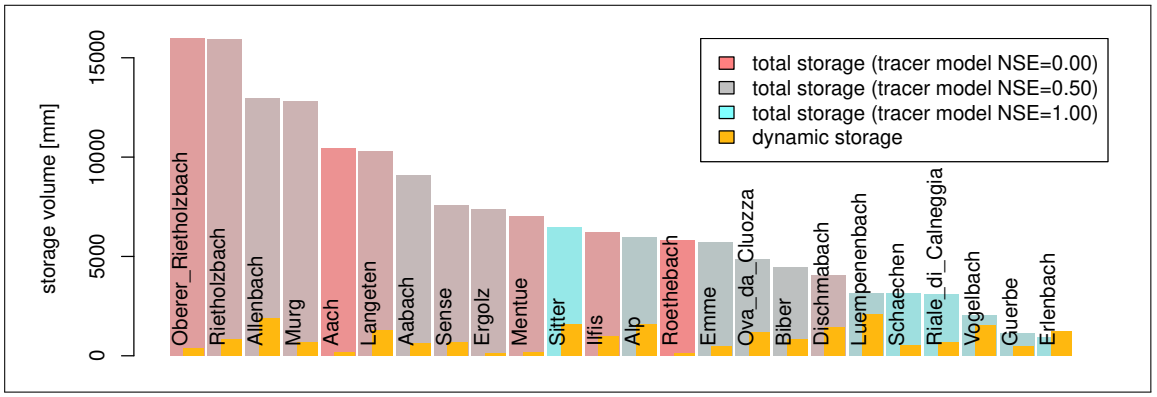

FIGURE 3.12: Total catchment storage and dynamic catchment storage estimates based on TPLR tracer models and TPLR hydraulic models. NSE actually is the median normalized NSE.

Chapter 4

Discussion

4.1 Calibration of precipitation and snow correction factors

The results presented in 3.3.2.1 suggest that the applied method to calibrate precipitation and snow correction factors described in 2.3.4.3 did not yield very reliable results. While the general height gradient is identifiable, some of the simulated values clearly lie outside of the plausible value range and have a high uncertainty. Apparently the simple precipitation correction calibration procedure in connection with the hardly identifiable parameters of the rainfall runoff module (see figure(A.1)) is not suited to obtain reliable estimates. However, according to the observed runoff values the original PREVAH-precipitation data clearly proved to underestimate the actual values for some, but not all of the higher located catchments without any precipitation correction. Therefore, the application of fix height dependant precipitation and snow correction factors also did not seem appropriate.

4.2 Tracer prediction bias

4.2.1 Possible reasons

The simulated runoff tracer concentrations for all catchments had a negative bias of at least -0.4, usually around -1 $\delta^{18}O$. Whilst there were minor differences between the

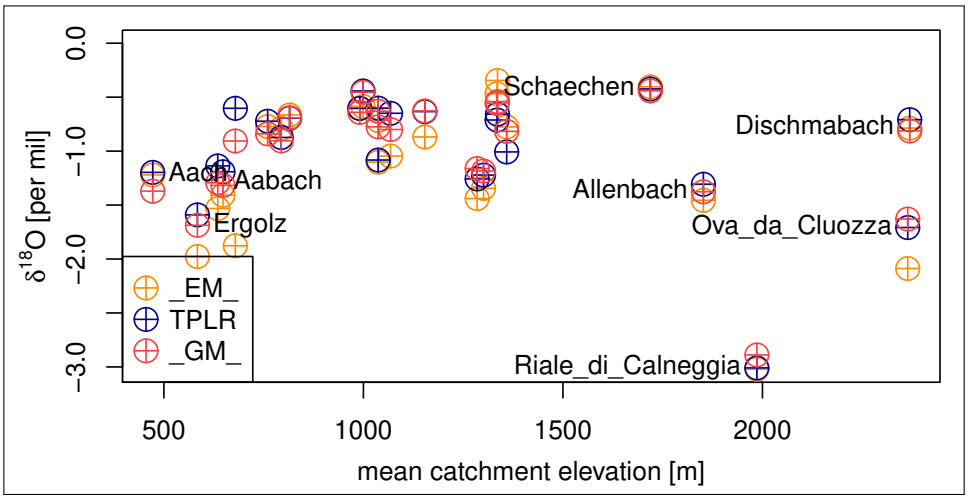

FIGURE 4.1: Comparison of tracer model prediction bias values plotted against mean catchment elevations. _EM_ is the exponential model, _GM_ the gamma distribution.

calibrated results for the different model types(see figure(4.1)), the bias values seem to be connected to the used model input data. The sparse input data measurement network is a source of uncertainty, especially at the borders of the study area and in regions with steep $\delta^{18}O$ gradients between stations. The most negative bias, with a value around -3 $\delta^{18}O$ was found for the catchment *Riale de Calneggia*. This catchment is located between the two ISOT-sites *Grimsel* and *Locarno*(see figure 2.4). From November to March, the $\delta^{18}O$ gradients between those two stations are very steep and their development is unclear. It is quite possible, that the $\delta^{18}O$ values for *Riale de Calneggia* are closer to the values measured in *Locarno* than *Grimsel*, as it lies south of the mountain ridges of the Swiss central Alps. Since the interpolation procedure described in 2.2.5) only considers elevations and does not account for topographic features, it simply computes the $\delta^{18}O$ values for *Riale de Calneggia* as a distance weighted mean of the values of mainly of *Locarno* and *Grimsel*, which might give the more negative $\delta^{18}O$ values of *Grimsel* too much weight. While similar cases might explain a part of the bias values, there is still no satisfying explanation for the fact, that all prediction bias values are negative. Even for the catchments located around the area where an independent evaluation of the predicted precipitation $\delta^{18}O$ values (see 3.2.2) was possible and did not indicate a bias show a consistent negative bias between 0.5 and 1.5 $\delta^{18}O$. This leads to the suggestion, that there might be a systematic error within the simulation.

One possible reason for the systematic negative $\delta^{18}O$ bias is the way the mean catchment values were modified during the height level wise data preprocessing (see 2.3.4.1). For

each height level the interpolated mean catchment elevation $\delta^{18}O$ value was changed according to a monthly (negative) $\delta^{18}O$ height gradient and weighted by the precipitation amount of the respective height level. As the precipitation amount tends to increase with height, the mean catchment $\delta^{18}O$ values were systematically decreased. Depending on the range of altitudes within a catchment and the precipitation gradients, this decrease ranged from below less than 0.1 up to -0.94 $\delta^{18}O$ in the simulations. Mueller et al. [2012], who conducted a study in the Swiss Ursern valley, reported that no $\delta^{18}O$ height gradient could be detected for the winter months, whilst Dietermann [2010] reported distinct height gradients for several catchments (amongst others *Dischmabach*) in the Swiss Alps. Another possible reason for the systematic negative $\delta^{18}O$ bias could lie in processes like throughfall enrichment(Dewalle and Swistock [1994]), which would lead to higher $\delta^{18}O$ in runoff compared to the precipitation's $\delta^{18}O$ values.
But even if there were absolutely no $\delta^{18}O$ height gradients within the catchments, which seems improbable, and enrichment processes should happen on a notable scale, what would lead to a change in Deuterium-Excess values (which could not be observed, see figure(3.1)), it would hardly be enough to eliminate the negative tracer prediction bias completely. Therefore, further investigation to explain this phenomenon is necessary.

4.2.1.1 Consequences

As a consequence of the biased input data, the objective function for the tracer model optimization had to be made insensible to any bias (by subtracting the respective median values of predicted and observed values before they were evaluated with the NSE), otherwise the optimization algorithm would to no avail have tried to eliminate the input data's bias and would have lost sight of the actual optimization. This attenuates the objective functions' usefulness as it might lead to good evaluations of parameter sets which result in biased predictions, even when the input data has no inherent bias.

4.2.1.2 Possible solution

If the observed runoff tracer concentration time series were long enough, it would be possible to determine the bias of the input precipitation data by comparison of longtime mean values for precipitation and runoff concentrations. Then the input data could be adjusted by this bias and a bias sensitive objective function could be used.

4.3 MTT estimates based on different transfer functions

4.3.1 Excursus: computation of the MTT for the TPLR

As far as known, Weiler [2003], McGuire [2005] and Hack [2010] did compute the MTTs for the TPLR (described in 2.3.1.4) numerically. In the source code used by Hack [2010], which is a modification of the source code of Weiler [2003], the numerical values computed for each timestep of the TPLR were normalized to yield a total sum of 1. Given a sufficiently big enough number of time steps and an agreement of time step length and the units used for the TPLR parameters τ_f and τ_s, such a normalization does nothing, as the TPLR transfer function integrates to unity anyway. In case the length of the numerical representation of the convolution function is not long enough to include the significant fraction of the convolution function, the normalization does in fact crop an essential part of the convolution function and redistributes the cropped fraction across the remaining fraction. This results in shorter MTT estimates than implied by the given parameters and the formula of the TPLR.

Example: For a simulation period from January 1998 to October 2005, Hack [2010] calibrated a TPLR-model to the $\delta^{18}O$ runoff values measured for the catchment *Brugga*. The calibration lead to the parameters: $\tau_f = 166.7$, $\tau_s = 1133.3$ and $\Phi = 0.06$. The numerical MTT computation for the according time series length yielded a value of 842 days. If the same computation procedure, using the same parameters, was applied over a much longer time period of 30 years, the resulting MTT would be 1075 days. Longer time series would not increase this value. The same, actual MTT value for the TPLR can be computed as:

$$\mathrm{MTT}_{\mathrm{TPLR}} = \Phi\tau_f + (1 - \Phi)\tau_s \tag{4.1}$$

The inaccuracy of the numerical MTT computation might be negligible, as long as τ_s is small and *Phi* (the fraction of the fast reservoir) is big enough. Otherwise the TPLR's convolution function has a very long tail, which is in danger to be cropped at the end of the simulation period. This might still lead to good simulation results. Though, as the cropped part is not discarded but, as a consequence of the normalization to unity, distributed across the remaining fraction of the convolution function, it can be argued that the computation is not sufficiently described by the TPLR's formula and parameters.

This makes it impossible to properly compare or reproduce results supposedly resulting from a given set of parameters and the formula of the TPLR.
The TPLR-model used in this study did not redistribute the cropped part of the convolution function but simply discarded it. MTTs for the TPLR were computed according to equation(4.1).

4.3.2 Comparability of MTTs from different transfer functions

As could be shown in 3.3.3.4, the MTT estimates depend significantly on the applied transfer function. It could be argued, that all estimated MTTs above 1/4 of the simulation period are too uncertain too be taken to into account, but even when only MTTs shorter than five years are considered, the differences between the model types are apparent. The different behaviour of the three transfer function shows, that a comparison of MTTs obtained by different transfer functions is problematic. Even when the simulated tracer concentration curves of different transfer functions are very similar and predict the observed values similarly good, the MTTs implied by the calibrated transfer function parameters can greatly differ. However, these assumptions are based on the available data for this study and it is possible that a similar study with longer runoff tracer concentration observation time series and more reliable precipitation tracer concentration data could show a higher agreement, at least between the TPLR and the gamma distribution transfer functions.

As already mentioned in 3.3.3.4, the MTTs for a series of catchments seem to roughly rank in the same order, when all are determined with the same transfer function, regardless which transfer function is used. For MTTs below two years, the estimates obtained by a TPLR model tend to be bigger than estimates obtained by a gamma distribution or exponential model. For longer MTTs, the exponential model tends to lose all predictive value, whereas gamma distribution and TPLR model are still able to reproduce the observed time series. However, while the MTTs implied by the TPLR model increase moderately, the MTTs implied by the gamma distribution model tend to grow much faster. This suggests, that the gamma distribution model has a limited temporal scope, but so does the application of seasonally fluctuating natural tracers.

4.4 Relations between MTTs and catchment characteristics

When the studied catchments are divided into two fractions: lower catchments with high MTTs located on the fissured sedimentary rock layers of the Swiss plateau and higher catchments with shorter MTTs on solid bedrock, no MTT height gradients or significant correlations to other topographic characteristics can be observed. Thus, the findings of McGuire [2005] could not be repeated, but it has to be noted, that the seven catchments studied by McGuire [2005] were located closely next to or within each other and the soils and underlying geology were very homogeneous. On the other hand, the 24 catchments in this study were distributed across a wide area and a notable range of altitudes with big differences in underlying geology. This suggests, that the influence of topographic characteristics on MTTs is smaller, than the influence of geological and climatic boundary conditions.

4.5 Evaluation of the estimated catchment storage volumes

With 392 mm, the lowest total storage volume estimate within this study was made with the exponential transfer function for the catchment *Erlenbach*. For the same catchment, the gamma distribution based estimate ranged from 380 to 610 mm. The lowest reported total storage volume which was found in the reviewed literature was 80 mm(McNamara et al. [2011]), but it was determined by a different method. Soulsby et al. [2011] stated storage estimates based on the gamma distribution transfer function between 300 and 2500 mm. However, the reason that the highest stated value was 2500 mm (with a MTT of 1275), is not that it actually was the highest value, but rather that the estimated MTTs of two catchments were considered too high (above 5000 days) to make a reliable storage estimate. Under the assumption that all these catchments had similar mean runoff values, there is no good reason to assume they had total storage volumes below 2500 mm, just because it is not certain how much above 2500 m they actually are). This means, that the total storage volumes of catchments with high MTT estimates might not be as high as implied by the products of MTTs and mean runoff values, but provided

the high MTT estimates resulted from simulations in agreement with the observations, there is a good chance that the total storage volumes are at least as high as the product of the mean runoff values and the highest acceptable MTT.

Chapter 5

Conclusions

The combination of an uncalibrated height distributed energy balance based snow model and a lumped parameter model, consisting of a non-linear rainfall loss module and a convolution model using the TPLR transfer function, managed to produce good runoff simulations for a set of catchments with different runoff regimes, different geological undergrounds and soil types. However, in some cases not all of the six parameters of the lumped rainfall-runoff model could be identified.

The comparison of the exponential model, the gamma distribution and the TPLR model as transfer functions for a lumped tracer concentration convolution model showed, that for MTTs above two years the TPLR and gamma distributions yielded better runoff tracer concentration predictions than the up to today most widely used exponential transfer function.

Compared to the estimated MTTs, the available tracer runoff concentration records for this study were very short. Therefore, the conclusion that TPLR and gamma distribution might imply significantly different MTTs for similar fits to the observed data cannot be made for sure.

Appendix A

Appendix A: rainfall-runoff model calibration

TABLE A.1: Calibration results for the rainfall loss module of Jakeman and Hornberger [1993] and the TPLR runoff model. Value ranges for average annual ETP and mean reaction times are given for 21 equally optimal simulations. The stated model parameters belong to the simulation with the median mean reaction time.

Catchment	Efficiency		ETP [mm/a]			mean reaction time [d]			rain fall loss module			TPLR runoff model		
	NSE	logNSE	median	min	max	median	min	max	c	τ[d]	f	τ_f [d]	τ_s [d]	Φ
Oberer_Rietholzbach	0.23	0.51	426	391	486	44	22	67	0.011	2.53	0.22	2.1	80	0.50
Vogelbach	**0.64**	0.26	503	474	602	64	46	85	0.015	1.21	0.16	1.2	164	0.59
Luempenenbach	**0.64**	0.57	265	190	377	56	40	69	0.019	1.88	0.18	1.3	176	0.70
Roethebach	**0.64**	**0.65**	762	735	800	27	13	51	0.008	3.95	0.07	2.4	63	0.60
Erlenbach	0.59	0.34	512	459	599	45	32	64	0.007	3.30	0.18	1.1	183	0.76
Aabach	**0.63**	**0.64**	704	682	756	64	39	93	0.011	2.24	0.11	2.2	160	0.59
Sitter	**0.66**	**0.67**	444	382	558	69	41	88	0.014	1.44	0.15	1.6	163	0.59
Murg	**0.73**	**0.70**	530	500	560	56	28	72	0.011	1.74	0.18	2.8	115	0.53
Sense	**0.70**	**0.72**	482	402	546	55	37	87	0.012	2.10	0.16	2.3	117	0.55
Ergolz	**0.67**	**0.79**	579	552	614	18	10	30	0.007	2.61	0.18	2.9	46	0.63
Allenbach	**0.68**	**0.65**	294	260	336	89	81	112	0.013	2.45	0.14	2.5	194	0.55
Aach	**0.62**	-1.80	586	542	634	22	14	48	0.009	1.92	0.18	2.5	64	0.68
Ova_da_Cluozza	**0.76**	**0.77**	306	260	336	81	63	106	0.010	2.66	0.13	3.2	148	0.43
Dischmabach	**0.81**	**0.84**	126	110	144	72	58	80	0.024	4.45	0.14	6.7	162	0.58
Langeten	**0.65**	**0.73**	581	557	617	126	96	156	0.011	2.21	0.12	2.6	172	0.26
Riale_di_Calneggia	**0.71**	**0.71**	688	615	815	41	32	48	0.013	1.26	0.09	1.8	95	0.58
Mentue	**0.67**	**0.75**	573	528	602	25	17	41	0.007	1.89	0.18	2.0	44	0.41
Emme	**0.65**	**0.71**	379	310	495	27	16	50	0.015	1.59	0.19	1.9	152	0.80
Rietholzbach	**0.66**	**0.63**	482	442	546	52	35	68	0.012	2.14	0.20	2.0	168	0.70
Guerbe	**0.71**	**0.71**	491	452	563	40	13	74	0.013	1.91	0.15	2.4	113	0.61
Schaechen	**0.79**	**0.87**	291	231	347	26	22	35	0.018	4.97	0.12	4.7	54	0.56
Ilfis	**0.69**	**0.71**	696	618	746	71	45	94	0.010	3.12	0.10	2.1	164	0.56
Biber	**0.65**	**0.68**	678	604	720	48	34	62	0.014	1.61	0.10	1.6	155	0.71
Alp	**0.68**	**0.68**	361	300	426	60	43	75	0.014	2.46	0.14	1.3	192	0.68

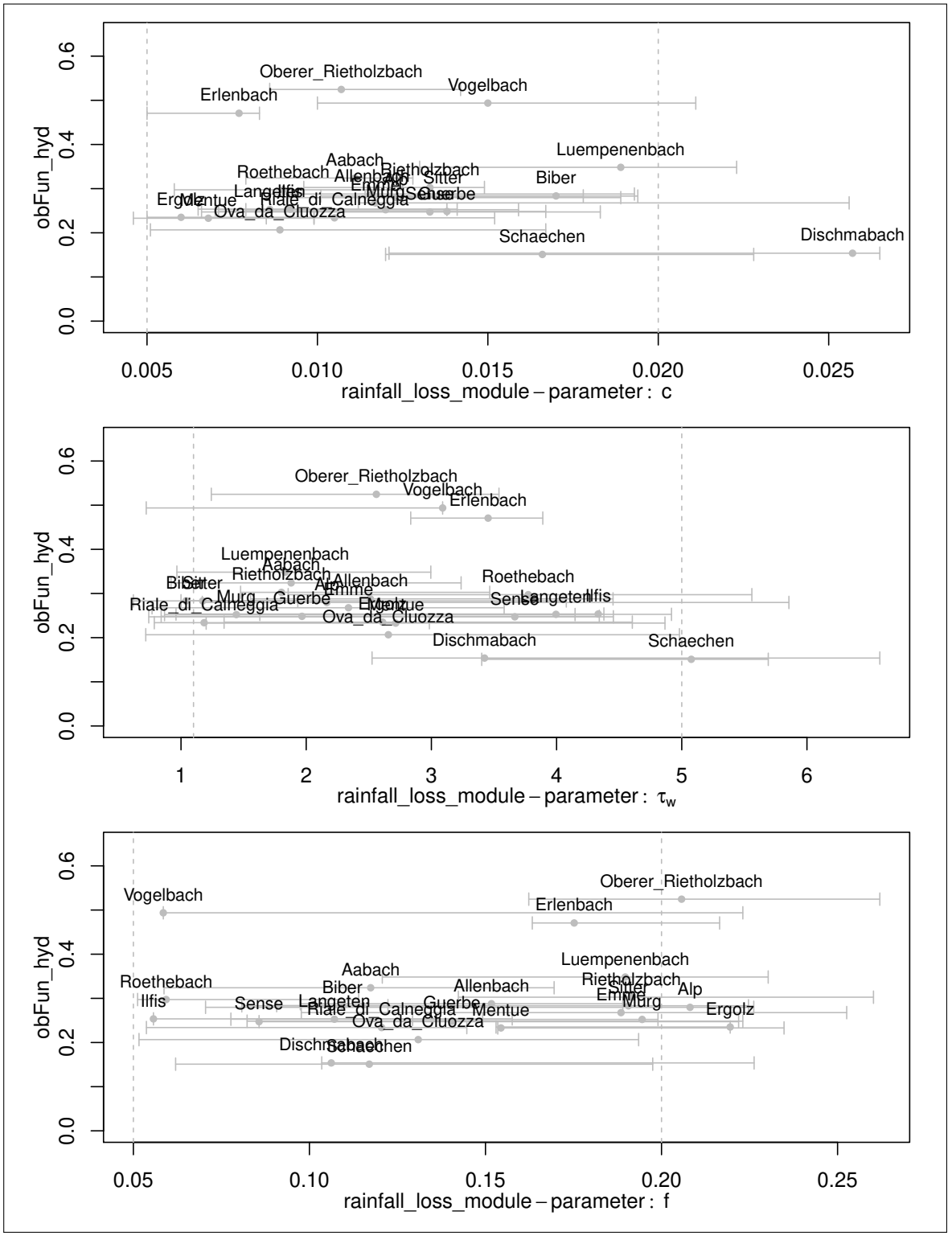

FIGURE A.1: Calibrated parameter values for the rainfall loss module after Jakeman and Hornberger [1993]. The grey dashed lines indicate the initial parameter bounds. Grey bars indicate the parameter values for 20 near to best simulations

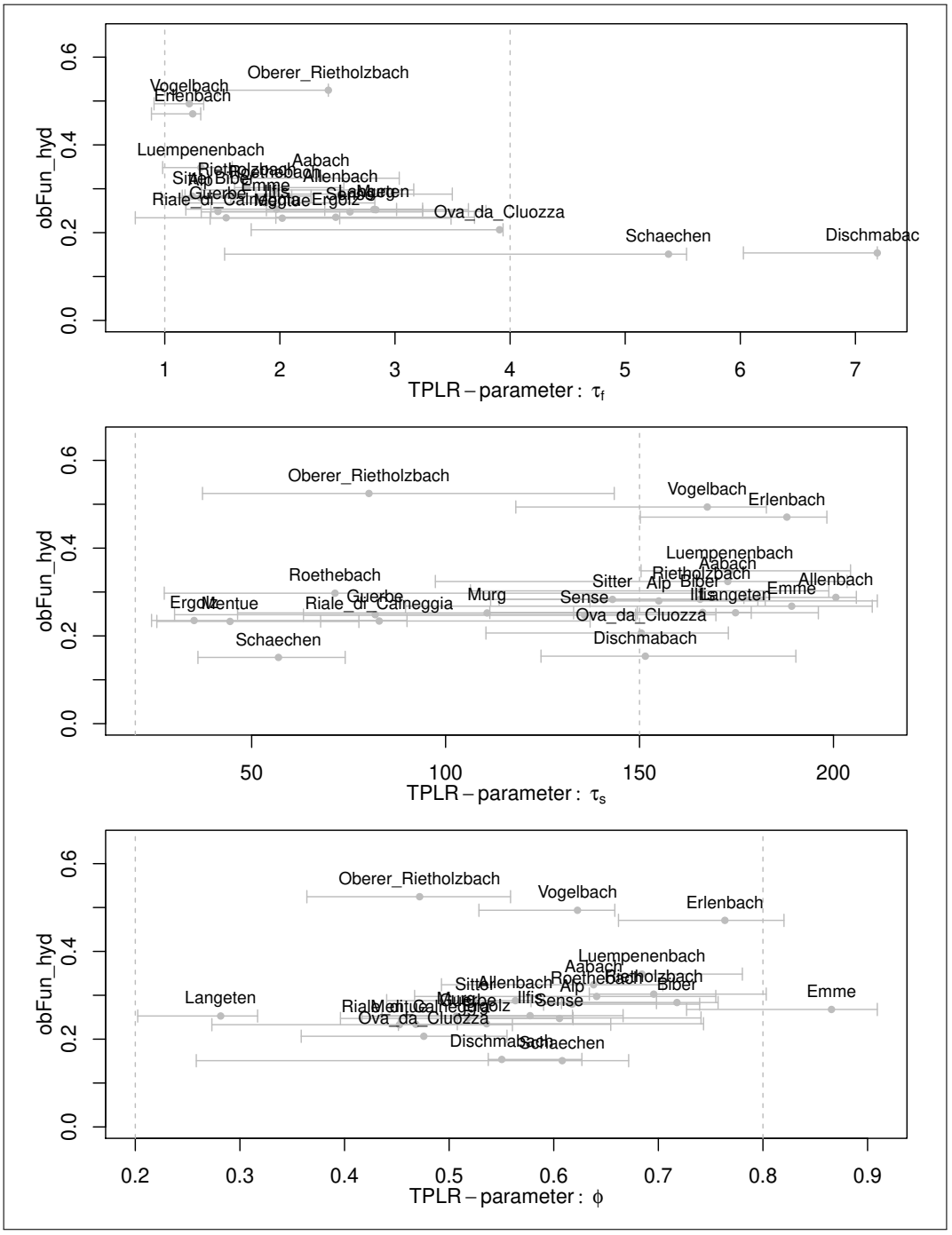

FIGURE A.2: Calibrated parameter values for the TPLR runoff models. The grey dashed lines indicate the initial parameter bounds. Grey bars indicate the parameter values for 20 near to best simulations

Appendix B

Appendix B

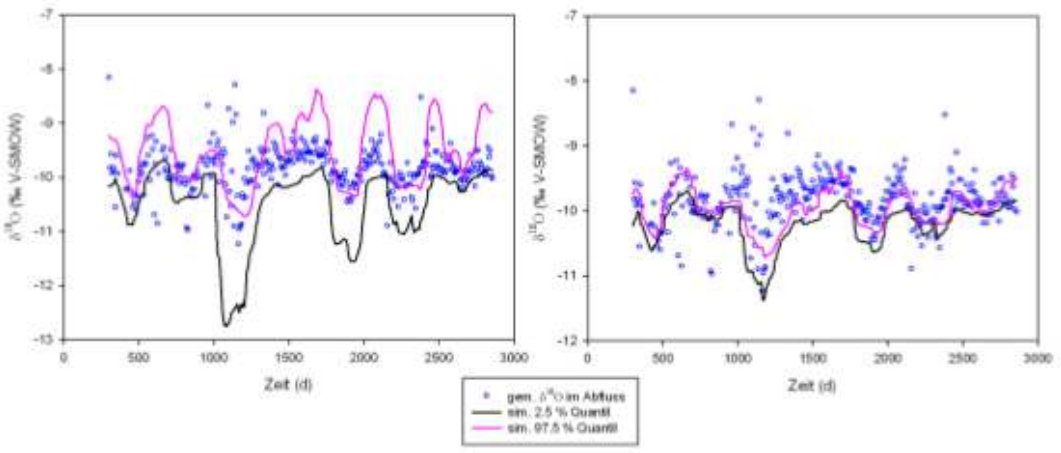

Abbildung 7.2.8: Gemessene und simulierte Isotopensignale im Abfluss für das Brugga-Einzugsgebiet für den Kalibrierzeitraum 1998-2005. links: Ergebnis der 1. Iteration. rechts: Ergebnis der 2. Iteration.

FIGURE B.1: This figure is taken from Hack [2010] and shows, that the ACO-stopping rule suggested by Abbaspour et al. [2001] can lead to a parameter range (indicated by the lines in the left figure) which is far more narrow than the 95% confidence interval it is supposed to represent

Bibliography

K. J. McGuire. The role of topography on catchment-scale water residence time. *Water Resources Research*, 41(5):W05002, 2005. ISSN 0043-1397. doi: 10.1029/2004WR003657. URL http://www.agu.org/pubs/crossref/2005/2004WR003657.shtml.

M. Hrachowitz, C. Soulsby, D. Tetzlaff, I. a. Malcolm, and G. Schoups. Gamma distribution models for transit time estimation in catchments: Physical interpretation of parameters and implications for time-variant transit time assessment. *Water Resources Research*, 46(10):W10536, October 2010. ISSN 0043-1397. doi: 10.1029/2010WR009148. URL http://www.agu.org/pubs/crossref/2010/2010WR009148.shtml.

C. Soulsby, K. Piegat, J. Seibert, and D. Tetzlaff. Catchment-scale estimates of flow path partitioning and water storage based on transit time and runoff modelling. *Hydrological Processes*, 25(25):3960–3976, December 2011. ISSN 08856087. doi: 10.1002/hyp.8324. URL http://doi.wiley.com/10.1002/hyp.8324.

M. H. Mueller, R. Weingartner, and C. Alewell. Relating stable isotope and geochemical data to conclude on water residence times in four small alpine headwater catchments with differing vegetation cover. *Hydrology and Earth System Sciences Discussions*, 9 (9):11005–11048, September 2012. ISSN 1812-2116. doi: 10.5194/hessd-9-11005-2012. URL http://www.hydrol-earth-syst-sci-discuss.net/9/11005/2012/.

Giorgos Kallis. Droughts. *Annual Review of Environment and Resources*, 33 (1):85–118, November 2008. ISSN 1543-5938. doi: 10.1146/annurev.environ.33.081307.123117. URL http://www.annualreviews.org/doi/abs/10.1146/annurev.environ.33.081307.123117.

Marc J. Leblanc, Paul Tregoning, Guillaume Ramillien, Sarah O. Tweed, and Adam Fakes. Basinscale, integrated observations of the early 21st century multiyear drought in southeast Australia. *Water Resources Research*, 45(4):W04408, April 2009. ISSN 0043-1397. doi: 10.1029/2008WR007333. URL http://www.agu.org/pubs/crossref/2009/2008WR007333.shtml.

B. Creutzfeldt, a. Güntner, S. Vorogushyn, and B. Merz. The benefits of gravimeter observations for modelling water storage changes at the field scale. *Hydrology and Earth System Sciences*, 14(9):1715–1730, September 2010. ISSN 1607-7938. doi: 10.5194/hess-14-1715-2010. URL http://www.hydrol-earth-syst-sci.net/14/1715/2010/.

Ole B. Andersen. GRACE-derived terrestrial water storage depletion associated with the 2003 European heat wave. *Geophysical Research Letters*, 32(18):2–5, 2005. ISSN 0094-8276. doi: 10.1029/2005GL023574. URL http://www.agu.org/pubs/crossref/2005/2005GL023574.shtml.

Benjamin F. Zaitchik, Matthew Rodell, and Rolf H. Reichle. Assimilation of GRACE Terrestrial Water Storage Data into a Land Surface Model: Results for the Mississippi River Basin. *Journal of Hydrometeorology*, 9(3):535–548, June 2008. ISSN 1525-755X. doi: 10.1175/2007JHM951.1. URL http://journals.ametsoc.org/doi/abs/10.1175/2007JHM951.1.

KJ McGuire and JJ McDonnell. A review and evaluation of catchment transit time modeling. *Journal of Hydrology*, pages 543–563, 2006. doi: 10.1016/j.jhydrol.2006.04.020. URL http://www.sciencedirect.com/science/article/pii/S0022169406002150.

Markus Weiler. How does rainfall become runoff? A combined tracer and runoff transfer function approach. *Water Resources Research*, 39(11):1315, 2003. ISSN 0043-1397. doi: 10.1029/2003WR002331. URL http://www.agu.org/pubs/crossref/2003/2003WR002331.shtml.

S. M. Dunn, C. Birkel, D. Tetzlaff, and C. Soulsby. Transit time distributions of a conceptual model: their characteristics and sensitivities. *Hydrological Processes*, 24(12):1719–1729, January 2010. ISSN 08856087. doi: 10.1002/hyp.7560. URL http://doi.wiley.com/10.1002/hyp.7560.

M. C. Roa-García and M. Weiler. Integrated response and transit time distributions of watersheds by combining hydrograph separation and long-term transit time modeling. *Hydrology and Earth System Sciences*, 14(8):1537–1549, August 2010. ISSN 1607-7938. doi: 10.5194/hess-14-1537-2010. URL http://www.hydrol-earth-syst-sci.net/14/1537/2010/.

Fabrizio Fenicia, Sebastian Wrede, Dmitri Kavetski, Laurent Pfister, Lucien Hoffmann, Hubert H. G. Savenije, and Jeffrey J. McDonnell. Assessing the impact of mixing assumptions on the estimation of streamwater mean residence time. *Hydrological Processes*, 24(12):1730–1741, February 2010. ISSN 08856087. doi: 10.1002/hyp.7595. URL http://doi.wiley.com/10.1002/hyp.7595.

Christian Birkel, Chris Soulsby, and Doerthe Tetzlaff. Modelling catchment-scale water storage dynamics: reconciling dynamic storage with tracer-inferred passive storage. *Hydrological Processes*, 25(25):3924–3936, December 2011. ISSN 08856087. doi: 10.1002/hyp.8201. URL http://doi.wiley.com/10.1002/hyp.8201.

James P. McNamara, Doerthe Tetzlaff, Kevin Bishop, Chris Soulsby, Mark Seyfried, Norman E. Peters, Brent T. Aulenbach, and Richard Hooper. Storage as a Metric of Catchment Comparison. *Hydrological Processes*, 25(21):3364–3371, October 2011. ISSN 08856087. doi: 10.1002/hyp.8113. URL http://doi.wiley.com/10.1002/hyp.8113.

S. L. Dingman. *Physical Hydrology*. Prentice Hall, New Jersey, 2002. ISBN 9780130996954.

H Craig. Standard for reporting concentrations of deuterium and oxygen-18 in natural waters. *Science (New York, NY)*, 17(1958):17–18, 1961. URL http://ukpmc.ac.uk/abstract/MED/17819002.

Bernward Hölting and Wilhelm Georg Coldewey. *Hydrogeologie - Einführung in die Allgemeine und Angewandte Hydrogeologie*. 2005.

W Dansgaard. Stable isotopes in precipitation. *Tellus*, 1964. URL http://onlinelibrary.wiley.com/doi/10.1111/j.2153-3490.1964.tb00181.x/abstract.

Christian Leibundgut, Piotr Maloszewski, and Christoph Külls. *Tracers in Hydrology*. John Wiley & Sons, Ltd, Chichester, UK, October 2009. ISBN 9780470747148. doi: 10.1002/9780470747148. URL http://doi.wiley.com/10.1002/9780470747148.

D. Viviroli, M. Zappa, J. Gurtz, and R. Weingartner. An introduction to the hydrological modelling system PREVAH and its pre- and post-processing-tools. *Environmental Modelling & Software*, 24(10):1209–1222, October 2009. ISSN 13648152. doi: 10.1016/j.envsoft.2009.04.001. URL http://linkinghub.elsevier.com/retrieve/pii/S1364815209000875.

JP Delhomme. Kriging in the hydrosciences. *Advances in water resources*, (5), 1978. URL http://www.sciencedirect.com/science/article/pii/0309170878900398.

Edzer J Pebesma. Multivariable geostatistics in S: the gstat package. *Computers & Geosciences*, 30(7):683–691, August 2004. ISSN 00983004. doi: 10.1016/j.cageo.2004.03.012. URL http://linkinghub.elsevier.com/retrieve/pii/S0098300404000676.

Sandy Hack. *Modellierungsstrategien und Auswertung der langjährigen Isotopenzeitreihe der Dreisam und Brugga*. PhD thesis, 2010.

AJ Jakeman and GM Hornberger. How much complexity is warranted in a rainfall-runoff model? *Water Resources Research*, 1993. URL http://coweeta.uga.edu/publications/1345.pdf.

MK Stewart and JJ McDonnell. Modeling base flow soil water residence times from deuterium concentrations. *Water Resources Research*, 27(10), 1991. URL http://watershed.montana.edu/oldhydrologyweb/PDFs/papers/StewartandMcDonnell_baseflowrestimes_WRR_1991.pdf.

P Malozewski and A Zuber. Determining the turnover time of groundwater systems with the aid of environmental tracers. *Journal of Hydrology*, 57:207–231, 1982. URL http://scholar.google.com/scholar?hl=en&btnG=Search&q=intitle:Determining+the+turnover+time+of+groundwater+systems+with+the+aid+of+environmental+tracers#1.

Jw Kirchner, X Feng, and C Neal. Fractal stream chemistry and its implications for contaminant transport in catchments. *Nature*, 403(6769):524–7, February 2000. ISSN 1476-4687. doi: 10.1038/35000537. URL http://www.ncbi.nlm.nih.gov/pubmed/10676956.

K C Abbaspour, R Schulin, and M Th Van Genuchten. Estimating unsaturated soil hydraulic parameters using ant colony optimization. 24, 2001.

JE Nash and JV Sutcliffe. River flow forecasting through conceptual models part IA discussion of principles. *Journal of hydrology*, 0, 1970. URL http://www.sciencedirect.com/science/article/pii/0022169470902556.

David R. Legates and Gregory J. McCabe. Evaluating the use of" goodness-of-fit" measures in hydrologic and hydroclimatic model validation. *Water Resources Research*, 35(1):233–241, 1999. URL http://www.agu.org/journals/wr/wr9901/1998WR900018/pdf/1998WR900018.pdf.

U. Strasser and T. Marke. ¡i¿ESCIMO.spread¡/i¿ a spreadsheet-based point snow surface energy balance model to calculate hourly snow water equivalent and melt rates for historical and changing climate conditions. *Geoscientific Model Development Discussions*, 3(2):627–649, May 2010. ISSN 1991-962X. doi: 10.5194/gmdd-3-627-2010. URL http://www.geosci-model-dev-discuss.net/3/627/2010/.

JE Sicart and JW Pomeroy. Incoming longwave radiation to melting snow: observations, sensitivity and estimation in northern environments. *Hydrological ...*, 3708:3697–3708, 2006. doi: 10.1002/hyp. URL http://onlinelibrary.wiley.com/doi/10.1002/hyp.6383/abstract.

Wilfried Brutsaert. On a derivable formula for long-wave radiation from clear skies. *Water Resour. Res.*, 11(5):742–744, 1975. ISSN 0043-1397. doi: 10.1029/WR011i005p00742. URL http://dx.doi.org/10.1029/WR011i005p00742.

RG Allen and LS Pereira. FAO Irrigation and drainage paper No. 56. *Rome: Food and ...*, (56), 1998. URL http://www.kimberly.uidaho.edu/water/fao56/fao56.pdf.

PV Unnikrishna, JJ McDonnell, and Carol Kendall. Isotope variations in a Sierra Nevada snowpack and their relation to meltwater. *Journal of Hydrology*, 260:38–57, 2002. URL http://www.sciencedirect.com/science/article/pii/S0022169401005960.

Nicolai Dietermann. *Stabile Isotope im Schnee : Räumliche und zeitliche Variabilität*. PhD thesis, 2010.

L Menzel. *Flächenhafte Modellierung der Evapotranspiration mit TRAIN*. 1999. URL http://www.pik-potsdam.de/research/publications/pikreports/.files/pr54.pdf.

Massimiliano Zappa and Joachim Gurtz. The Spatial Resolution of Physiographic Data as Sensitive Variable for Distributed Hydrological Simulations in Prealpine and Alpine Catchments. *wsl.ch*, 2001. URL ftp://ftp.wsl.ch/pub/zappa/publications/conference_papers/icwrer_mz_2002b.pdf.

DR Dewalle and BR Swistock. Differences in oxygen18 content of throughfall and rainfall in hardwood and coniferous forests. *Hydrological Processes*, 8(August 1992):75–82, 1994. URL http://onlinelibrary.wiley.com/doi/10.1002/hyp.3360080106/abstract.